A global model-measurement evaluation of particle light scattering coefficients at elevated relative humidity

M.A. Burgos[1,2], E. Andrews[3], G. Titos[4], A. Benedetti[5], H. Bian[6,7], V. Buchard[6,8], G. Curci[9,10], A. Kirkevåg[11], H. Kokkola[12], A. Laakso[12], M. Lund[13], H. Matsui[14], G. Myhre[13], C. Randles[6], M. Schulz[11], T. van Noije[15], K. Zhang[16], L. Alados-Arboledas[4], U. Baltensperger[17], A. Jefferson[3], J. Sherman[18], J. Sun[19], E. Weingartner[17,20], and P. Zieger[1,2]

[1]Department of Environmental Science and Analytical Chemistry, Stockholm University, Stockholm, Sweden
[2]Bolin Centre for Climate Research, Stockholm, Sweden
[3]Cooperative Institute for Research in Environmental Studies, University of Colorado, Boulder, USA
[4]Andalusian Institute for Earth System Research, University of Granada, Granada, Spain
[5]European Centre for Medium-Range Weather Forecasts, Reading, UK
[6]NASA/Goddard Space Flight Center, USA
[7]University of Maryland Baltimore County, Maryland, USA
[8]GESTAR/Universities Space Research Association, Columbia, USA
[9]Dipartimento di Scienze Fisiche e Chimiche, Universita' degli Studi dell'Aquila, L'Aquila, Italy
[10]Centre of Excellence CETEMPS, Università degli Studi dell'Aquila, L'Aquila, Italy
[11]Norwegian Meteorological Institute, Oslo, Norway
[12]Finnish Meteorological Institute, Kuopio, Finland
[13]Center for International Climate Research, Oslo, Norway
[14]Graduate School of Environmental Studies, Nagoya University, Nagoya, Japan
[15]Royal Netherlands Meteorological Institute, De Bilt, Netherlands
[16]Earth Systems Analysis and Modeling, Pacific Northwest National Laboratory, Richland, WA, USA
[17]Laboratory of Atmospheric Chemistry, Paul Scherrer Institute, Villigen, Switzerland
[18]Department of Physics and Astronomy, Appalachian State University, Boone, USA
[19]Key Laboratory of Atmospheric Chemistry of CMA, Chinese Academy of Meteorological Sciences, Beijing 100081, China
[20]Now at: Institute for Sensing and Electronics, University of Applied Sciences, Windisch, Switzerland

Correspondence: M.A. Burgos (maria.burgos@aces.su.se) and P. Zieger (paul.zieger@aces.su.se)

Abstract. The uptake of water by atmospheric aerosols has a pronounced effect on particle light scattering properties which in turn are strongly dependent on the ambient relative humidity (RH). Earth system models need to account for the aerosol water uptake and its influence on light scattering in order to properly capture the overall radiative effects of aerosols. Here we present a comprehensive model-measurement evaluation of the particle light scattering enhancement factor f(RH), defined as the particle light scattering coefficient at elevated RH (here set to 85 %) divided by its dry value. The comparison uses simulations from 10 earth system models and a global dataset of surface-based in situ measurements. In general, we find a large diversity in the magnitude of predicted f(RH) amongst the different models which can not be explained by the site types. There is strong indication that differences in the model parameterizations of hygroscopicity and perhaps mixing state are driving at least some of the observed diversity in simulated f(RH). An important finding is that the models show a significantly larger discrepancy with the observations if RH_{ref}=0 % is chosen as the model reference RH compared to when RH_{ref}=40 % is used. The multi-site average ratio between model outputs and measurements is 1.64 in the former case and 1.16 in the latter. The overestimation by

1

the models is believed to originate from the hygroscopicity parameterizations at the lower RH range which may not implement all phenomena taking place (i.e. not fully dried particles and hysteresis effects). Our results emphasize the need to consider the measurement conditions in such comparisons and recognize that measurements referred to as 'dry' may not be dry in model terms.

5   1   Introduction

The effects of aerosol particles on the climate system are well known and appear as a consequence of the aerosol-radiation interaction (i.e., by scattering or absorption of solar radiation), the aerosol-cloud interaction (when aerosols act as cloud condensation nuclei or ice nuclei and thereby change cloud microphysical and radiative properties; IPCC, 2013), and the rapid adjustments of aerosol-radiation interaction (when aerosols change the cloud cover by heating the atmosphere where clouds
10   reside; see e.g., Bond et al., 2013). Atmospheric aerosol particles are critical forcing agents in the climate system and, despite the increased number of studies in recent years, aerosol forcing remains (together with clouds) the largest uncertainty in climate change predictions (e.g., Ramanathan et al., 2001; IPCC, 2013; Regayre et al., 2018).

Aerosol optical properties, such as the wavelength-dependent light scattering coefficient, $\sigma_{\mathrm{sp}}(\lambda)$, are often measured under dry conditions (relative humidity (RH) below 40 %), as recommended by international protocols (e.g., WMO/GAW, 2016).
15   However, aerosol particles can undergo hygroscopic growth and their optical properties are different at ambient conditions. The response of an aerosol particle to the surrounding RH is dependent on its size and solubility. Aerosol optical properties are thus dependent on RH: water uptake modifies particle size and chemical composition (and thus the complex refractive index) and this, in turn, affects the aerosol optical properties.

The scattering enhancement factor, $f(\mathrm{RH}, \lambda)$, is a key parameter that describes the change in particle light scattering coefficient
20   $\sigma_{\mathrm{sp}}(\lambda)$ as a function of RH:

$$f(\mathrm{RH}, \lambda) = \frac{\sigma_{\mathrm{sp}}(\mathrm{RH}, \lambda)}{\sigma_{\mathrm{sp}}(\mathrm{RH_{dry}}, \lambda)}. \tag{1}$$

$f(\mathrm{RH}, \lambda)$ typically increases with increasing RH and is larger than 1 if particles do not experience significant restructuring when taking up water (Weingartner et al., 1995). The scattering enhancement factor is a way to represent aerosol hygroscopicity and its direct effect on particle light scattering.
25   There have been multiple measurement-based studies focused on investigating the scattering enhancement factor measured at different sites around the globe; Titos et al. (2016) compared $f(\mathrm{RH}, \lambda)$ at many of these as a function of dominant aerosol type. In general, they showed that clean marine aerosols exhibit higher $f(\mathrm{RH}, \lambda)$ than is measured at sites with anthropogenic influence, consistent with other studies (Wang et al., 2007; Fierz-Schmidhauser et al., 2010a; Zieger et al., 2013). In addition to $f(\mathrm{RH}, \lambda)$ as a function of dominant aerosol type, more detailed investigations have also been done. Zieger et al. (2010) analyzed
30   aerosol water uptake using nephelometer measurements of wet and dry scattering coefficient, aerosol size distribution, and Mie theory at the Arctic site Ny-Ålesund. Svalbard. At Melpitz (a rural site in Germany), Zieger et al. (2014) found a correlation

between the scattering enhancement factor and the aerosol chemical composition, in particular the inorganic mass fraction. Results from seven years of aerosol scattering hygroscopic growth measurements at the rural Southern Great Plains site in the USA indicated higher growth rates in the winter and spring seasons, which correlated with a high aerosol nitrate mass fraction (Jefferson et al., 2017). Burgos et al. (2019) created an open access database of scattering enhancement factors for 26 sites,

covering a wide range of aerosol types whose optical properties were measured both long-term and as part of field campaigns. An accurate estimation of aerosol effects on climate by Earth system models (ESMs) requires a realistic representation of aerosols (aerosol size distribution, mixing state, and composition).[1] Models must also be able to simulate processes in the aerosol life cycle such as primary emissions, new particle formation, coagulation, condensation, water uptake, and activation to form cloud droplets among others. Representing aerosol processes and properties in ESMs poses a great challenge due to the diversity and complexity of atmospheric aerosols. ESMs have implemented special modules and treatments for aerosols and the estimates of aerosol radiative forcing and climate impacts will be influenced by the uncertainties associated with the description of these processes. However, a compromise must be achieved between sufficiently representative aerosol and atmospheric process representations and the resultant computational cost (Ghan et al., 2012).

The effect of harmonized emissions on aerosol properties in global aerosol models was analyzed by Textor et al. (2007), who found that the aerosol representation is controlled, to a large extent, by processes other than the diversity in emissions. This implied that the harmonization of aerosol sources has only a small impact on the simulated inter-model diversity of the global aerosol burden and optical properties. Results are largely controlled by model-specific representation of transport, removal, chemistry and aerosol microphysics.

Previous model studies have suggested that water associated with aerosol particles can lead to significant differences amongst model predictions. For example, Zhang et al. (2012) demonstrated that there are significant differences in simulated aerosol water content due to changes in a model's scheme to predict water uptake. Myhre et al. (2013) explored direct aerosol radiative forcing from a suite of models, showing that the primary source of differences among model predictions of the mass extinction coefficient was aerosol hygroscopic growth of sulfate aerosols. Haywood et al. (2008) used tandem-humidifier nephelometer measurements from an aircraft to assess the parameterization of aerosol water uptake by the Met Office Unified Model. They found that ambient aerosols were simulated as being too hygroscopic as a result of being modeled as composed solely of ammonium sulfate.

The Aerosol Comparison between Observations and Models (AeroCom) project (Textor et al., 2006; Schulz et al., 2006; Kinne et al., 2006, https://aerocom.met.no) aims to analyze global aerosol simulations to enhance understanding of aerosol particles and their impact on climate. In this project, intercomparisons among global aerosol models and comparisons with observations of aerosol properties have been carried out. These types of model evaluations allow for the identification of sources of model diversity and determination of which modeled aerosol properties need improvement. The objective of tier III of the INSITU measurement comparison experiment within AeroCom phase III (https://wiki.met.no/aerocom/phase3-experiments),

---

[1]Note that we are here using the more general term of Earth System Model, while keeping in mind that other definitions (e.g. global climate models, general circulation models, transport models, etc.) are commonly used as well.

is to assess how well model simulations represent observations of aerosol water uptake by comparing a high-quality, long-term, in situ measurements dataset with the output of several global aerosol models and that is what was done here.

2   Measurements

In this study, measured particle light scattering enhancement factors, $f(\mathrm{RH}, \lambda)$, from 22 different sites covering a wide range
of site types (Arctic, marine, rural, mountain, urban and desert) are used. Note that all results here will be shown for λ=550 nm;
λ will be omitted in the equations and variable names and only mentioned when necessary. Table 1 summarizes the station
location and acronyms, while Fig. S1 (in supplementary material) shows a map with the location of these sites, color-coded
by site type. The $f(\mathrm{RH})$ measurement data comes from the openly available scattering enhancement dataset described by
Burgos et al. (2019). Four sites from Burgos et al. (2019) dataset were excluded in this current analysis, either because they
10 had a small upper size cut (PM_1 or $\mathrm{PM}_{2.5}$, i.e., particulate matter with aerodynamic diameters less than 1 or 2.5 μm) or a
very low number of data points (N<10). This scattering enhancement dataset was developed from dry and wet particle light
scattering measurements made as part of field campaigns and long-term monitoring efforts by the USA Department of Energy
Atmospheric Radiation Measurements (DoE/ARM), the USA National Oceanic and Atmospheric Administration Federated
Aerosol Network (NOAA-FAN, Andrews et al., 2019), the Swiss Paul Scherrer Institute (PSI), and/or the Chinese Academy
15 of Meteorological Sciences (CAMS).

The scattering coefficients were measured simultaneously under two different conditions: first, under so-called dry or low-RH
conditions (namely RH<40 %, from here on called $\mathrm{RH}_{\mathrm{ref}}$) with a reference nephelometer or DryNeph, and secondly, scanning
over a programmable range of RH values, mainly between 40 and 95 %, with a second humidified nephelometer or WetNeph
(Sheridan et al., 2001; Fierz-Schmidhauser et al., 2010b). The wide range of scanned RH values were typically achieved by
20 passing the aerosol particles through a humidifier system before they entered the WetNeph. One possible limitation of this
approach could be that the sample air may not equilibrate if the residence time in the elevated relative humidity downstream
of the humidifier is too short (Sjogren et al., 2007). However, the measurements performed by PSI at the European sites JFJ,
MHD, CES and MEL (see summary in Zieger et al., 2013) and HYY (Zieger et al., 2015) were all accompanied by optical
closure studies using Mie theory together with measured size distribution and chemical composition and/or hygroscopic growth
25 factors, which revealed no apparent bias due to too short residence times inside the WetNeph.

In order to create a benchmark dataset for aerosol scattering enhancement, an identical process for data treatment was applied
to all initial raw scattering coefficients, and data quality was assured by a thorough inspection of the scattering time series for
each site (Burgos et al., 2019). The final dataset is composed of yearly files organized in three levels, containing scattering
coefficients, hemispheric backscattering coefficients, and scattering enhancement factors for three wavelengths (450, 550, and
30 700 nm) and two particle size cuts (aerodynamic diameters lower than 10 and 1 μm). Level 1 contains the raw scattering data,
Level 2 the corrected scattering coefficients and calculated scattering enhancement factors, and Level 3 contains the calculated
$f(\mathrm{RH}$=85 %/ $\mathrm{RH}_{\mathrm{ref}})$. A detailed description of the data screening process and the corrections applied, the specific wavelengths

and size cuts at each site, as well as the design and characteristics of the different instrument systems are given in Burgos et al. (2019) and references therein.

One of the strengths of the dataset is that it was developed using a homogenized data treatment - differences in data processing was one of the issues cited in Titos et al. (2016) hygroscopicity overview paper that limited absolute comparisons of f(RH)

5   values reported in the literature. The homogenized data treatment facilitates the intercomparison of the stations included in the dataset as well as the comparison against global model output. In this study, we use Level 2 f(RH=85 %/RH$_\mathrm{ref}$=40 %) at $\lambda = 550$ nm data from 22 stations (those with PM$_{10}$ size cut or whole-air measurements) (see Table 1 for information about the station names, IDs, and aerosol types). The dry value of particle light scattering coefficient used to retrieve the scattering enhancement factor can be a) measured with the DryNeph at any RH$_\mathrm{ref}$<40 %, or b) extrapolated to exactly RH$_\mathrm{ref}$=40 %. We first

10   present the model-measurement comparison results using DryNeph RH values extrapolated to RH$_\mathrm{ref}$=40 %. This is followed by a discussion on the implications of making different assumptions about the DryNeph RH value for both measurements and models.

3   Models

In this section, we present the ten models used in this study. We first provide a brief description of their main characteristics

15   and relevant references, where detailed information on each model's parameterizations/assumptions can be found. The models used are: Community Atmosphere Model version 5 (CAM5), Aerosol Two-dimensional bin module for foRmation and Aging Simulation (CAM-ATRAS), the CAM5.3-Oslo (CAM-OSLO) model, the Goddard Earth Observing System with the MERRA Aerosol Reanalysis (GEOS-MERRAero), the Georgia Institute of Technology-Goddard Global Ozone Chemistry Aerosol Radiation and Transport model (GEOS-GOCART), the GEOS-Chem (GEOS-Chem) model, the Tracer Model (TM5), the Oslo

20   chemistry-transport model (OsloCTM3), the European Centre for Medium-Range Weather Forecast - Integrated Forecasting System model (ECWMF-IFS) run in the Copernicus Atmosphere Monitoring Service configuration, and the global general circulation model ECHAM6 with the SALSA module (ECHAM6.3-SALSA2.0). For simplicity, we will refer to these models as: CAM, ATRAS, CAM-OSLO, GEOS-Chem, GEOS-GOCART, MERRAero, TM5, OsloCTM3, IFS-AER, and SALSA, respectively.

25   CAM5.3, CAM-ATRAS, and CAM-OSLO make use of the same general circulation model, the Community Atmosphere Model (CAM5.3). Three more models (GEOS-Chem, GEOS-GOCART and MERRAero) use the Goddard Earth Observing System assimilated meteorological fields. Table 2 summarizes some of the most relevant characteristics of each model, such as parameterizations of hygroscopic growth, meteorology, mixing states, species and size bins. The model data used in this study were provided within the AeroCom phase III experiments and are composed of aerosol absorption and extinction coefficients

30   at RH = 0, 40, and 85 %. Model values of scattering coefficient were obtained by subtracting absorption coefficient from extinction coefficient. The models were run for the year 2010 and data from 22 locations (closest gridpoint to the observational data) have been extracted. Exact temporal collocation between measurements and models can only be achieved at three of the measurement sites (BRW, GRW, and SGP), which made measurements in 2010. The model output files provide data at either

1h, 3h, or daily resolution, while the measurement data is primarily at hourly resolution with some of the more pristine sites averaged to six-hourly resolution (see Tables 1 and 2 for details).

3.1 CAM5

CAM5.3 is one of the versions from the CAM family models used in this study. The run we work with provided data at
5   surface level with a grid resolution of 1.9º latitude x 2.5º longitude, and at hourly frequency. CAM5.3 uses the modal aerosol module which provides a compromise between computational resources and a sufficiently accurate representation of aerosol size distribution and mixing states. However, depending on the selected number of modes and aerosol species in each mode, it can still incur differences among models. This model uses the version with three lognormal modes, MAM3, which is described in detail in Liu et al. (2012b). As a brief description, MAM3 has Aitken, accumulation and coarse modes and it assumes
10 that: a) primary carbon is internally mixed with secondary aerosol, b) coarse dust and sea salt modes are merged, c) fine dust and sea salt modes are similarly merged with the accumulation mode, and d) sulfate is partially neutralized by ammonium. Hygroscopicity is based on κ-Köhler theory and the values used for the different aerosol components are listed in Table S3 of Liu et al. (2012b).

To represent the meteorological field, the nudging technique (Newtonian relaxation) has been used, with horizontal winds
15 nudged towards ERA-Interim reanalysis, following Zhang et al. (2014). The present day (year 2000) anthropogenic emissions are prescribed using CMIP5 emission data (IPCC, 2013). Natural wind-driven aerosol (dust and sea salt) emissions are calculated online. CAM5.3 accounts for the following important processes that influence aerosols: nucleation, coagulation, condensational growth, gas- and aqueous-phase chemistry, emissions, dry deposition and gravitational settling, water uptake, in-cloud and below-cloud scavenging, and production from evaporated cloud and rain droplets. Details on the representation
20 of these processes can be found in the supplemental material of Liu et al. (2012a).

3.2 CAM-ATRAS

In this case, the CAM model is used but the aerosol module is changed to the Aerosol Two-dimensional bin module for foRmation and Aging Simulation (ATRAS). The run we work with provided data at surface level with the same grid resolution (1.9º latitude x 2.5º longitude) as CAM5.3, and at hourly frequency. Meteorological nudging was used for temperature and
25 wind fields in the free troposphere (<800 hPa) by using the MERRA2 (Modern-Era Retrospective Analysis for Research and Applications) data.

This model takes into account the following aerosol processes: primary aerosol emissions, gas- and aqueous-phase chemistry, nucleation, condensation and evaporation, secondary organic aerosols processes, dry and wet deposition, aerosol activation to cloud droplets and water uptake. In this study, aerosol particles from 1 to 10 μm in dry diameter are represented with 12 size
30 bins for sulfate, ammonium, nitrate, sea salt, dust, organic aerosol, and black carbon. The aerosol module as well as details and references for the aerosol processes treatment can be found in Matsui et al. (2014); Matsui (2017) and Matsui and Mahowald (2017). Related to to water uptake, κ-Köhler theory is used with the hygroscopicity parameter κ for each species given in Matsui (2017).

3.3 CAM-OSLO

In this case, the aerosol module OsloAero5.3 is applied in the atmosphere model CAM5.3 model, which runs with a grid resolution of 0.9º latitude x 1.25º longitude. A thorough description and general modelling and validation results from this aerosol module used in the atmospheric component CAM5.3-Oslo of the Norwegian Earth System Model (NorESM1.2) have been published (Kirkevåg et al., 2018).

For aerosols, the model represents sulfate, black carbon, primary and secondary organic aerosols, sea salt and mineral dust. The following processes are taken into account: nucleation, coagulation, condensational growth, gas- and aqueous-phase chemistry, emissions, dry deposition and gravitational settling, water uptake, in-cloud and below-cloud scavenging, and cloud processing. Unlike (e.g.) MAM3, this aerosol module makes use of a "production tagged" method to calculate aerosol size and chemical composition. It describes a number of "background" log-normal modes that can change their size distribution due to condensation, coagulation, and cloud processing. A detailed offline size-resolving model carries out the corresponding aerosol micro-physical calculations, and a selection of results are stored in lookup tables. Hygroscopicity is estimated for each particle size and type by the volume mixing ratios, adding (by condensation) water as a function of RH according to Köhler theory. In CAM-OSLO, optical parameters are found by interpolation in look-up tables at the actual RH in each grid-box and time. The model data is output at hourly frequency.

3.4 GEOS-Chem

GEOS-Chem is a community global three-dimensional Eulerian chemistry-model originally described in (Bey et al., 2001) with updates that are described in http://acmg.seas.harvard.edu/geos/geos_chem_narrative.html (last accessed 28 November 2019). Here we use version 10-01 of the model. GEOS-Chem is driven by assimilated meteorological observations from the Goddard Earth Observing System (GEOS) of the NASA Global Modeling and Assimilation Office (GMAO). For this work, we use the GEOS fields version 5.2.0 degraded from the native resolution to the 2° x 2.5° simulation grid and 47 levels, for computational expediency. For anthropogenic emissions we use EDGAR 4.2 complemented with regional inventories where available (US, Canada, Mexico, Europe and East Asia).

The aerosol module employs a bulk mass approach for sulfate-nitrate-ammonium system and for black carbon and organic aerosol. Soil dust and sea salt are simulated with a sectional approach having four and two size bins, respectively. The aerosol optical properties are calculated from the simulated aerosol mass assuming log-normal size distribution with parameters taken from OPAC (Optical Properties of Aerosols and Clouds, Hess et al., 1998) and updated by Jaeglé et al. (2011) and Heald et al. (2014), adopting an external mixing representation. The hygroscopic growth factors are taken from Chin et al. (2002).

3.5 GEOS-GOCART

The Goddard Chemistry, Aerosol, Radiation, and Transport module (GOCART) (Chin et al., 2002, 2009) was implemented in the NASA GEOS global Earth system model to simulate aerosol processes of sources, sinks, transport, and transformation (Colarco et al., 2010; Bian et al., 2013, 2017). For this study, the aerosol species included are sulfate, dust, organic carbon

(OC), black carbon (BC), and sea salt. The model is "replayed" from the MERRA meteorological analyses at the same spatial resolution produced by the NASA Global Modeling and Assimilation Office (Rienecker et al., 2011). Every 6 h the model dynamical state (winds, pressure, temperature, and humidity) is set to the balanced state provided by MERRA and then a 6 h forecast is performed until the next analysis is available. The GEOS model is run with a grid resolution of 0.5º latitude x 0.625º longitude and with 72 vertical layers from surface up to 0.01 hPa (about 85 km). Aerosols are considered to have different degrees of hygroscopic growth with ambient RH (with the exception of dust). The hygroscopic growth follows the equilibrium parameterization of Gerber (1985) for sea salt and OPAC (Hess et al., 1998) for other aerosols.

3.6 GEOS-MERRAero

The GEOS Earth System Model is a weather- and climate-capable model which includes atmospheric circulation and composition, as well as oceanic and land components. This model includes the same aerosol transport module based on the GOCART (Chin et al., 2002; Colarco et al., 2010) that is used in the previously described GEOS-GOCART. The specific version of GEOS used in this study also includes assimilation of bias-corrected Aerosol Optical Depth (AOD) from the Moderate Resolution Imaging Spectroradiometer (MODIS) sensors. This is the so-called MERRAero aerosol reanalysis (Buchard et al. (2015)). Driven by the MERRA meteorology, MERRAero was run at a global 0.5 x 0.625 latitude-by-longitude horizontal resolution with 72 vertical layers and 3-hour frequency. The data assimilation step provides a direct observational constraint on the simulated 550 nm AOD, but absorption, speciation and vertical distribution remain largely driven by the background simulation. Optical properties of the aerosols are primarily based on Mie calculations using the particles properties as in Chin et al. (2002) and Colarco et al. (2010) with spectral refractive indices and hygroscopic growth parameterizations primarily from the OPAC database (Hess et al., 1998). The Gerber growth curve (Gerber, 1985), is used for sea salt.

3.7 TM5

The Tracer Model 5 (TM5) is an atmospheric chemistry and transport model. The version used for this study is an update of the model described by van Noije et al. (2014). Essentially the same version was used to carry out the Tier I experiment of the INSITU project in 2016. For the study presented here, additional diagnostics were included in the model to assess the hygroscopic growth at varying relative humidity.

TM5 uses a regular grid with a horizontal resolution of 3º longitude x 2º latitude and 34 vertical levels. At high latitudes, the number of grid cells in the zonal direction is gradually reduced towards the poles. Dry deposition velocities and the emissions of DMS, sea salt and mineral dust are calculated on a 1º x 1º surface grid, and subsequently coarsened to the atmospheric grid. The hygroscopic growth of the soluble modes follows the description in Vignati et al. (2004). For pure sulfate-water particles the water uptake is calculated using the parameterization from (Zeleznik, 1991). When sea salt is present in the soluble accumulation or coarse modes, the water uptake is calculated using the ZSR method (Stokes and Robinson, 1966; Zdanovskii, 1948). Below relative humidities of 45 %, sea salt is assumed to be dry. Additional water uptake in the presence of ammonium-nitrate in the soluble accumulation mode is calculated using EQSAM (Metzger et al., 2002). BC, OA and dust do not influence the water uptake. For calculating the aerosol optical properties at relative humidities other than ambient conditions, additional

diagnostic calls to M7 and EQSAM have been included to calculate the water uptake in the relevant modes at these RH values. Apart from the water content, all other aerosol components are kept at their levels calculated at ambient conditions.

3.8   OsloCTM3

OsloCTM3 is a chemistry-transport model, described in detail in Lund et al. (2018). The model includes several updates with regards to its predecessor, OsloCTM2, particularly in the convection, advection, proto-dissociation, and scavenging schemes. OsloCTM3 is a global three-dimensional transport model that is driven by 3h offline meteorological forecast data from IFS ECMWF and CEDS emissions as described in Hoesly et al. (2018). With respect to aerosols, it includes BC, primary and secondary organic aerosols, sulfate, nitrate, dust and sea salt and its aerosol module is inherited from OsloCTM2, with the main updates described in Søvde et al. (2012) and Lund et al. (2018). The hygroscopic growth for sulfate, nitrate and sea salt follows Fitzgerald (1975), and for organic aerosols from fossil fuel emissions and of secondary origin from Peng et al. (2001), and finally Magi and Hobbs (2003) for biomass burning aerosols, see further description in Myhre et al. (2007). The run used in this study has a grid resolution of 2.25º latitude x 2.25º longitude and daily frequency output was provided.

3.9   IFS-AER

The European Centre for Medium Range Weather Forecasts (ECMWF) model uses the Integrated Forecasting System aerosol module (IFS-AER), which is described in Morcrette et al. (2009), and an update regarding its parameterizations for aerosol sources, sinks and chemical production is provided in Rémy et al. (2019). The aerosol configuration is run operationally by the Copernicus Atmosphere Monitoring Service to provide daily aerosol analyses and 5-day forecasts. In this configuration, the model runs with a grid resolution of 0.5º latitude x 0.5º longitude. The data files provided have 3h frequency. Hygroscopic growth follows the description of Bozzo et al. (2019) for sulfates, sea salt and organic matter. This includes the parameterization of Tang (1997) for sea salt, and Tang and Munkelwitz (1994) for sulfates. The species taken into account are sea salt, desert dust, hydrophilic and hydrophobic OM, and BC and sulfate.

3.10   SALSA

SALSA is the sectional aerosol module that has been coupled to the ECHAM-HAMMOZ aerosol-chemistry-climate model framework. The model version used in this study was ECHAM6.3-HAM2.3-MOZ1.0. The detailed description of SALSA along with the details of its implementation and evaluation against several types of observations have been presented by Kokkola et al. (2018). The SALSA module describes aerosol size distribution with 10 size classes in size space which include two parallel externally mixed size classes for insoluble and soluble aerosol, thus tracking 17 size classes covering dry diameters from 3 nm to $10\,\mu$m. It simulates all relevant atmospheric aerosol processes including aerosol-cloud interactions. Simulated compounds are sulfate, organic carbon, black carbon, sea salt, dust and water. The hygroscopic growth in SALSA is calculated according to the Zdanovskii-Stokes-Robinson (ZSR) equation described in Stokes and Robinson (1966) assuming that the

soluble fraction of particles is always in liquid phase. Simulations were run with T63 spectral resolution (approx 1.9º latitude x 1.9º longitude), with 47 vertical levels and hourly output frequency.

4   Results

In this section we present the results showing the comparison between in situ measurements and the ten models described in
the previous sections. We first provide a general comparison of scattering enhancement measured at 22 sites in the Burgos
et al. (2019) dataset with model outputs. For this analysis, temporal collocation of model and measurement data is made on a
climatological basis. Hourly model output for the simulation year 2010 will be selected only from those months where hourly
measurement data is available (regardless of the year the measurements were made). In a second step, we perform a more
detailed analysis for three sites that did measure during 2010, and thus allow an exact temporal collocation with the models,
collocating for the time, day, and month of the year 2010. Finally, we explore how assumptions about 'what is dry' impact the
f(RH) values and the model-measurement comparisons.

4.1   Comparison of modeled vs. measured f(RH)

Figure 1 shows the box and whisker plots of the particle light scattering enhancement factor f(RH=85 %/RH$_{ref}$=40 %), where
the dry reference RH is taken at RH$_{ref}$=40 %, for both the measurements and models. Note that models CAM-OSLO and
MERRAero have fewer extracted sites (18 and 21, respectively) than the available measurement stations. These models pro-
vided data extracted at site locations, rather than the full global simulation and four station locations (CBG, FKB, HLM, and
LAN) were not requested from CAM-OSLO at the time of their model run and one (LAN) was not requested from MERRAero
at the time of their run. The box edges represent the 25th and 75th percentiles, with a line for the median (50th percentile).
The whiskers shows the range of the data expanding from the percentile 10th to the 90th. The gray shaded area indicates the
range of the 25th to 75th percentiles of the measurements and is plotted to facilitate comparison with the modeled values.
The number of measurements for each individual site have been added in the top right corner of the plots. As noted above,
the model statistics shown represent the same time period as the measurements, but the measurement year may not match the
model year. For example, MHD has measurements during January and February of 2009, so model data shown for MHD has
been restricted to January and February (but from 2010). The sites are organized by site type: Arctic (BRW, ZEP), marine
(CBG, GRW, GSN, MHD, PVC, PYE, THD), mountain (JFJ), rural (APP, CES, FKB, HLM, HYY, LAN, MEL, SGP), urban
(HFE, PGH, UGR) and desert (NIM).

In general, the top 10 panels (Fig. 1 a-j), comprising the Arctic, marine and mountain sites, and the desert site (Fig. 1 v) tend
to exhibit the best agreement among the models and the measurements (i.e., more models fall within the shaded area). These
sites tend to be the furthest away from local sources and may be more representative of a larger area. Two sites (CBG and
PVC) both on the north-eastern coast of North America (CBG is in Nova Scotia and PVC in coastal Massachusetts) are less
well simulated; in both cases the models tend to simulate larger scattering enhancement than is observed. Titos et al. (2014)
showed that there were significant differences in f(RH) at PVC depending on whether the sample air was urban influenced or

predominantly marine. The rural and urban sites (Fig. 1 k-u) tend to exhibit lower scattering enhancement than is simulated by the models. In this second group, the sites CES and MEL are the exception, with most of the models falling in the shaded area, and, for MEL, occasionally below the shaded area.

Overall, high variability among the models is observed. The CAM-family models (ATRAS, CAM, and CAM-OSLO) exhibit differences among themselves and also, in general, large variability of f(RH) values within each model. In contrast, the three GEOS models (GEOS-Chem, GEOS-GOCART and MERRAero) and OsloCTM3 exhibit similar predicted scattering enhancement values for all three models and a quite narrow variability within each model. TM5 and SALSA exhibit the largest variability within their results, as can be seen at some rural (e.g., APP, CES, HYY, and SGP) and urban sites (HFE, PGH, and UGR). IFS-AER, on the other hand, simulates very little variability in f(RH) for urban and rural sites and underestimates the f(RH) at the vast majority of sites.

In general, most of the models tend to overestimate f(RH) at almost all site types, except for the IFS-AER model which shows a general underestimation. There are several sites that most models (except IFS-AER) consistently overestimate, for example: CBG, APP, FKB, HYY, LAN, PGH and UGR. For some sites this may be due to complex topography and emissions sources. For example, Granada (UGR) is surrounded and impacted by desert dust from the Saharan desert and black carbon originating from local emissions (e.g., traffic and biomass burning, Titos et al., 2017). Similarly, PGH is in the foothills of the Himalayan range and is influenced by local and transported aerosol plumes (Dumka et al., 2017), and LAN is a polluted background station representative of the Yangtze River Delta conditions, influenced by anthropogenic emissions and dust (Zhang et al., 2015). For other sites, model overestimates may be due to other factors such as modeled chemistry or size distribution. It is beyond the scope of this paper to bring measurements of aerosol microphysical and chemical properties into the analysis, but that is a topic intended for future work.

Figure 2 shows the mean and standard deviations of the modeled versus measured f(RH=85 %/RH$_{ref}$=40 %) for each model, color-coded by site type. The one to one relationship is indicated by a solid black line and the gray dashed lines represent 30 % uncertainty bounds which is the maximum uncertainty of the measurements as described in Burgos et al. (2019). ATRAS, TM5 and SALSA exhibit a tendency to overestimate f(RH), while IFS-AER tends to underestimate f(RH). The figure also shows a wide diversity between modeled and measured f(RH) for the different models. For example, the CAM-family models and TM5 exhibit a wider range in f(RH) relative to the GEOS-family models and IFS-AER, which exhibit very little range in f(RH). The narrow range of f(RH) is also noticeable for the IFS-AER model but with a shift towards lower values (between 1.2 and 1.5), in accordance with the general underestimation of this model as discussed above.

The GEOS-family models all use GADS by Köpke et al. (1997) (or OPAC by Hess et al., 1998, which uses essentially the same values) to parameterize hygroscopicity. This simplified aerosol property model provides size and hygroscopic growth parameters of six components (for various size ranges) at selected RH values, where models often use linear interpolation. Zieger et al. (2013) have shown that OPAC can be problematic for modeling hygroscopicity as it results in an overestimate of f(RH) at low RH. However, such an overestimate would not necessarily explain the small range in modeled f(RH) for the models using it. Another commonality among the GEOS-family models, and IFS-AER as well, is that they assume an external mixing state. Aerosol optical properties calculated from bulk aerosol models which assume external mixing may be

inherently different from the optical properties calculated from more detailed microphysical models which assume internal mixing. SALSA, however, also assumes an externally mixed aerosol but does not exhibit the narrow range in f(RH) seen for the other models making this assumption.

The other models mostly fall within the 30 % interval of (upper) measurement uncertainty estimate (Burgos et al., 2019). CAM and OsloCTM3 are the models that most accurately estimate f(RH) at all site types, with the simulated results falling closest to the 1:1 black line and being within the 30 % interval. The Pearson correlation coefficient is also shown in the left top corner of each panel. The best correlations are found for OsloCTM3 and CAM ($r = 0.71$), followed by TM5 ($r = 0.65$). The GEOS-family models have correlation coefficients close to 0.5, while IFS-AER and SALSA show negative correlation with the measurements.

As shown in Fig. 1, the Arctic and desert sites appear to be the most accurately simulated sites, as almost all predicted model values lie within the 30 % interval area. CAM, OsloCTM3 and TM5 (and to a lesser extent CAM-OSLO) appear to replicate the observed pattern of the Arctic and marine sites having higher f(RH) than other sites, although CAM and TM5 both overestimate the observed Arctic and marine f(RH) values. ATRAS and SALSA are similar in that they tend to simulate higher f(RH) values for marine and rural sites and lower for Arctic locations, with ATRAS predicting the highest hygroscopicity at rural sites. The GEOS-family and IFS-AER do not exhibit a large enough range in simulated f(RH) to determine if some site types are more hygroscopic than others.

4.2 Investigating the importance of temporal collocation at BRW, GRW, and SGP

Temporal collocation of model data with observational data is an important aspect in model-measurement evaluation exercises (Schutgens et al., 2016). The model runs were conducted to simulate the year 2010 and three sites provide data covering almost that entire year. These sites exhibit distinct differences in their prevalent aerosol type: BRW, an Arctic site, GRW, a marine site, and SGP, a rural site. Temporal collocation has been carried out by selecting only those model data sampled at the same hours (days for OsloCTM3 and GEOS-GOCART models) with valid measurement data.

Figure 3 shows, in the left column, the annual cycle (monthly medians) of the scattering enhancement factor for f(RH=85 % / RH$_{\text{ref}}$=40 %). The black lines represent the observations (solid line: year 2010 only, dashed line - all available measurements, gray area represents the quartiles of all measurements), and the colored lines the predictions by the different models. The observations from 2010 do not show obviously different characteristics compared to the climatology of the entire dataset for each site. The exception is the latter half of the year at BRW where the 'all data' climatology is $\sim$12 % lower than the 2010 values. The variability in the measured monthly f(RH) is significantly narrower than the range of f(RH) simulated by the models, suggesting exact collocation in time will have a limited impact on the overall model-measurement comparison. Using all data allows extension of the comparison to additional months which were not covered in 2010.

Measurements at GRW and SGP do not exhibit a marked seasonal cycle in f(RH), while the seasonal cycle appears to be much larger for BRW, with larger values occurring in the second half of the year. Most of the models (CAM, CAM-OSLO, GEOS-Chem, GEOS-GOCART, MERRAero, OsloCTM3, and IFS-AER) do not capture the observed monthly variations. SALSA exhibits monthly variations similar to measurements at both BRW and GRW, while TM5 performs best at capturing the

monthly variations (but not the magnitude) at the three sites (see Fig. S2 in supplemental materials). ATRAS shows pronounced variations in the annual cycle of $f(\text{RH})$, with particularly large values in January-February and November-December which are not observed in the measurements. This modeled seasonality (or lack thereof) is easier to quantify using Taylor diagrams as discussed below.

5   To the right of each annual cycle plot in Fig. 3 there is a Taylor diagram (Taylor, 2001) showing the skill of the models for these three sites when the model results are collocated both in time and space with the measurements. Taylor diagrams are used to provide a concise statistical summary on how well models match measurements in terms of standard deviation (represented by the radial distances from the origin to the points) and correlation coefficient (represented by the angle from the normal). Black symbols represent the in situ measurements and colored symbols represent the different models in our study. The correlation

10   coefficients are quite low, suggesting that the models do not capture the monthly variability seen in the measurements. The correlation coefficients are lower than 0.25 for GRW and SGP for all models. The highest correlation (r=0.38) is observed for BRW by the GEOS-GOCART model while other models exhibit less correlation with the BRW $f(\text{RH})$ observations. Negative correlation coefficients are also found for some models at the three sites.

   The models exhibit a fairly wide range of standard deviations (between 0.1 and $\sim$0.7, depending on model and site), with SD

15   values both above and below the SD observed for the models. The standard deviation (SD) of the measurements is largest ($>$0.4) for CAM and TM5 at the three sites. The Taylor diagrams suggest a lack of skill in the models at simulating the seasonality and variability of observed aerosol hygroscopicity even when the data are exactly temporally collocated.

4.3   The importance of defining the dry reference RH

   Based on recommendations from WMO/GAW (WMO/GAW, 2016), experimentalists try to maintain sampling conditions

20   for 'dry' aerosol optical properties at RH$<$40 % and, as a first approximation, consider RH values below 40 % to be 'dry'. Measurements at dry conditions enables a comparison of aerosol properties across locations while minimizing the confounding effects of water. Making measurements at low RH is not without issues. Changing the conditions of the aerosol from ambient to RH$<$40 % can potentially result in the loss of volatile species such as nitrate and some organics (Bergin et al., 1997). Further, depending on the site environment, it can be difficult to maintain the sample conditions such that RH$_{\text{ref}}<$40 % (see Fig. S3 in

25   the supplementary material). In fact, seasonal changes in ambient temperature and ambient RH can be reflected in the resulting measurement RH.

   Complicating the picture is that some types of aerosol particles (e.g., sea salt, sulfuric acid or organic aerosol) will take up water at RH values below 40 %. Figure 4 provides a selection of the scattering enhancement as a function of RH for five sites covering multiple airmass types in Europe (based on Fig. 5 from Zieger et al., 2013). At all of these sites the $\sigma_{\text{sp}}(\text{RH}_{\text{dry}})$

30   was maintained at RH$<$30 % and often less than 20 %. These curves, obtained using tandem nephelometer humidograph measurements demonstrate that as RH increases, $f(\text{RH})$ has a tendency to also increase for almost all airmass types depicted. This is true even below RH=40 %. Further, the plots show that $f(\text{RH})$ depends on aerosol type, with cleaner and/or maritime air masses typically exhibiting higher enhancements than more polluted air masses. The magnitude of the enhancement at relatively low RH can be significant, for example, the humidogram for a non-sea salt event measured in the Arctic (see blue

curve in Fig. 4 marked by an arrow) shows that particle light scattering increases by approximately 25 % due to water uptake at $RH_{ref} = 40\%$ relative to dry scattering. For the sea salt event at the same site (dark blue line with markers), the hygroscopic growth is lower, but still observable. The water uptake at low RH even by pure inorganic sea salt has been confirmed by several independent methods (see Fig. S4).

5   When modelers are asked to provide simulations of aerosol optical properties at dry conditions, they typically will provide output at RH=0%. Depending on model assumptions about aerosol hygroscopicity and the types of aerosol particles studied, this can create large discrepancies between modeled and measured estimates of aerosol hygroscopicity. While the previous discussion has focused on comparisons with model simulations at RH=40 % and measurements with RH_{ref} extrapolated to 40 %, it is useful/instructive to evaluate the impact of comparing the choice of RH_{ref}=0 % with that of RH_{ref}=40 %.

10 Figure 5 demonstrates the impact of the choice of reference RH (RH_{ref}) on the comparison of observations and models. The figure shows the probability distribution function of the ratio between the modeled and measured $f(RH)$, for each model for two RH_{ref} conditions. Each distribution takes into account all sites and the full periods of measurements, calculating the ratios between the model monthly median values of $f(RH)$ and the monthly median $f(RH)$ values for each site. A ratio larger than one appears for those models that tend to overestimate measurements.

15 The blue distributions in Fig. 5, which are for reference RH_{ref}=40 %, summarize the data that have been shown in the previous two sections. For most models, the peak of the blue curve is near, but above 1, indicating relatively good agreement between models and measurements, albeit with a slight bias toward higher hygroscopicity than is observed. The IFS-AER curve maximum is below 1, as expected based on the earlier observations that the IFS-AER model tends to underestimate hygroscopicity. The high variability in simulated $f(RH)$ observed for TM5 and ATRAS is reflected in the width of the histograms for those

20 two models, while the low variability for some other models is indicated by narrow histograms.
The gray distribution in Fig. 5 represents the $f(RH)$ model-measurement ratio where RH_{ref}=0 % (for the model) and RH_{ref} is at dry conditions (for the measurements), meaning measurement RH_{ref} can be any value below 40 % - whatever the actual measurement condition was (see Fig. S3). Model overestimation is found to be larger when RH_{ref} is set to 0 % for the GEOS-family models (GEOS-Chem, GEOS-GOCART, MERRAero) and SALSA and, to a lesser extent, for ATRAS and CAM-OSLO.

25 The ratio of the modeled $f(RH)$ to measured $f(RH)$ when RH_{ref}=0 % is 1.64, and it decreases to 1.16 when using RH_{ref}=40 %. The implication is that the models that exhibit such large differences between RH_{ref}=0 % and RH_{ref}=40 % conditions are simulating significant hygroscopic growth between 0-40 % RH. Such growth would often not be seen by the measurements because the measurements are rarely (if ever!) that dry. In contrast, CAM, TM5 and IFS-AER exhibit very little difference in their $f(RH=0\%)$ and $f(RH=40\%)$ histograms. This suggests these three models assume little growth below RH=40 %. In

30 particular, MAM in CAM model assumes that if RH<35 % the aerosol particles have fully crystallized (are in solid state) and have not taken up water. As with the distribution for RH_{ref}=40 %, the only model showing underestimation of measurements for RH_{ref}=0 % is IFS-AER. This underestimation is larger if RH_{ref} is 40 % (ratio of 0.74 for RH_{ref}=40 % and 0.88 for RH_{ref}=0 %). The comparison presented in Fig. 5 highlights the differences in the model hygroscopicity parameterizations at the lower RH range (e.g. not fully dried particles and hysteresis effects). The discrepancy in $f(RH)$ for the two RH_{ref} conditions presented in

35 Fig. 5 is consistent with the hygroscopic growth simulated between RH=0 and 40 % (i.e., $f(RH=40\%/RH=0\%)$), shown in Fig.

S5. This finding is further supported by the minimal shift in the $f(\mathrm{RH})$ probability distribution function when the two $\mathrm{RH_{ref}}$ values are considered (Fig. S6).

This difference between the comparison at $\mathrm{RH_{ref}}=0\,\%$ and $\mathrm{RH_{ref}}=40\,\%$ may also explain the results of Gliss et al. (2019) (to be submitted at the same time to ACP, Dec. 2019). They performed model/measurement comparisons for both in situ scattering and aerosol optical depth (AOD). For their in situ scattering comparison, 'dry' scattering measurements were compared with model simulations reported at RH=0 %; they found that the ensemble model value underestimated the observed scattering by 33 %. In contrast, for the AOD comparisons, which were at ambient conditions for both models and measurements, the ensemble model value underestimated only by approximately 20 % (10-33 % depending on the source of AOD data). Thus, Gliss et al. (2019)'s larger model underestimate for in situ scattering than AOD may be due, at least in part, to the disconnect between the model and measurement definition of 'dry', although obviously other factors may also play a role. The results from this study and Gliss et al. (2019) imply that models would need to simulate higher aerosol loads and surface concentrations (or higher mass extinction coefficients) along with a reduced f(RH) to reduce the overall bias between models and measurements. This type of comparison demonstrates the usefulness of evaluating models against a variety of independent atmospheric observations - here it suggests further exploration of the role of hygroscopic growth across a range of RH values is warranted.

5 Conclusions

This works presents the first comprehensive model-measurement evaluation exercise for aerosol hygroscopicity and its effect on light scattering (22 sites, 10 Earth System Models). Model simulations of $f(\mathrm{RH})$ for the year 2010 were compared to spatially collocated measurements. The models exhibited large variability and diversity in the simulated $f(\mathrm{RH})$, but tended to overestimate $f(\mathrm{RH})$ relative to the measurements (with the exception of the IFS-AER model) when $\mathrm{RH_{ref}}=40\,\%$. The mean ratio between modeled $f(\mathrm{RH})$ and measurements is 1.16 (0.74 for IFS-AER). The GEOS-family models and IFS-AER tend to simulate a narrow range of $f(\mathrm{RH})$ relative to the other models - possibly related to use of the GADS parameterization and/or mixing state (although other unconsidered model assumptions may also be relevant). The models did not capture the weak annual cycle of observed $f(\mathrm{RH})$ at three sites representing distinct regimes (polar, rural, and marine) when it was possible to also temporally collocate the observations.

Agreement between models and measurements was strongly influenced by the choice of $\mathrm{RH_{ref}}$. Better agreement between observations and models is found when $\mathrm{RH_{ref}}=40\%$. In addition, some models exhibited unexpectedly large differences in $f(\mathrm{RH})$ at low RH (i.e. modeled scattering enhancement was significantly different for $\mathrm{RH_{ref}}=0\,\%$ and $\mathrm{RH_{ref}}=40\,\%$), pointing to the sensitivity in the model parameterization of hygroscopic growth at low RH (e.g. effects of particle hysteresis). To address this for future evaluations, models and measurements should be compared at similar RH conditions. For example, models could calculate the values at the same variable conditions as the measurements, although that would be computationally more intensive since measurement conditions can vary with site and season. Alternatively, if measurements could better control their reference RH, both keeping it below 40% and maintaining a narrower distribution of $\mathrm{RH_{ref}}$, there would be less uncertainty in the model/measurement comparisons. Caution must always be taken when changing the measurement conditions - semivolatile

species may volatilize with decreasing RH, inducing a negative artifact. While such losses are known and characterized for some species such as ammonium nitrate, we are still far away from a quantitative understanding such effects for semi-volatile organic species.

Based on the results presented here there are several topics that should be explored. One is to evaluate whether the gamma fit parameter is a more robust indicator for model/measurement comparisons than $f(\text{RH})$. Doing so would require model and measurement scattering data over a range of RH conditions. Another avenue is related to the $f(\text{RH})$ dependence on both chemical composition of the particles and particle size. Measured chemistry and size data collocated with scattering enhancement measurements at the sites where that information is available could be used to assess modeled simulations of these factors and their impact on modeled scattering enhancement. Finally, another challenging task on the measurement side is to measure the scattering at RH > 85 % (e.g., 90-100 %) where the steepest hygroscopic growth happens and where models introduce large diversity in f(RH) due to assumptions on sub-grid scale humidity fluctuations and cloud versus cloud-free conditions.

Author contributions. M.B. performed the model-measurement evaluation. M.B., E.A., G.T., and P.Z. designed study and wrote the paper. A.B., H.B., V.B., G.C., A.K., H.K., A.L., H.M., G.M., C.R., N.S., T.N. and K.Z. designed and performed model calculations. L.A., U.B., A.J., J.S., J.S., E.W., G.T., and P.Z. provided measurement data. All authors read and commented on the manuscript.

Competing interests. The authors declare no competing interests.

6 Tables

Table 1. General site information. The median RH_{ref} refers to the relative humidity inside the (dry) reference nephelometer, while the temporal resolution refers to measured values of f(RH). More details and references on the sites can be found in Burgos et al. (2019).

Station ID	Station Name, Country	Latitude (º)	Longitude (º)	Site Type	Median RH_{ref} (%)	Temporal Resolution (h)
BRW	North Slope of Alaska, USA	71.3	-156.6	Arctic	6.8	6
ZEP	Zeppelin, Norway	78.9	11.9	Arctic	11.6	6
JFJ	Jungfraujoch, Switzerland	46.6	8	Mountain	5.2	3
CBG	Chebogue Point, Canada	43.8	-66.1	Marine	28.2	1
GRW	Graciosa, Portugal	39.1	-28	Marine	28.5	1
GSN	Gosan, S. Korea	33.28	126.2	Marine	33.0	1
MHD	Mace Head, Ireland	53.3	-9.9	Marine	26.4	3
PVC	Cape Cod, USA	42.1	-70.2	Marine	24.0	1
PYE	Point Reyes, USA	38.1	-123	Marine	28.9	1
THD	Trinidad Head, USA	41.1	-124.2	Marine	28.8	1
APP	Appalachian State, USA	36.2	-81.7	Rural	13.6	1
CES	Cabauw, Netherlands	52	4.9	Rural	13.3	3
FKB	Black Forest, Germany	48.5	8.4	Rural	21.5	1
HLM	Holme Moss, UK	53.5	-1.9	Rural	27.6	1
HYY	Hyytiälä, Finland	61.9	24.3	Rural	28.2	3
LAN	Lin'an, China	30.3	119.7	Rural	12.2	1
MEL	Melpitz, Germany	51.4	12.9	Rural	10.7	3
SGP	Southern Great Plains, USA	36.6	-97.5	Rural	18.3	1
HFE	Shouxian, China	32.6	116.8	Urban	22.4	1
PGH	Nainitial, India	29.4	79.5	Urban	30.4	1
UGR	Granada, Spain	37.2	-3.6	Urban	15.9	1
NIM	Niamey, Niger	13.5	2.2	Desert	9.4	1

Table 2. Summary of main characteristics implemented by each model. Model main reference, general hygroscopic growth (hygroscopic growth for marine aerosols), meteorology, mean RH value (subgrid variability considered), mixing state (black carbon), and species (number of size bins). In Hygroscopic growth column: GADS = Global Aerosol DataSet. g(RH) refers to the hygroscopic growth factor defined as the wet divided by the dry particle diameter. In Meteorology column: GMAO = Global Modeling and Assimilation Office. In Mixing State column: E = external, I = internal. In Species and size bins column: BC = black carbon, OA = organic aerosol.

Model (temporal resolution)	Main Reference	Hygroscopic Growth (for marine aerosols)	Meteorology	Mean RH (subgrid variability)	Mixing State	Species (size bins)
ATRAS (1h)	Matsui (2017)	κ-Köhler Theory (κ=1.16 for sea salt at RH=90 %)	Nudged to MERRA	clear-sky (no)	I	sulfate, nitrate, ammonium, BC, OA, dust, sea salt (12)
CAM (1h)	Liu et al. (2012b)	κ-Köhler Theory (κ=1.16 for sea salt at RH=90 %)	Nudged to ERA interim	clear-sky (no)	I	species: sulfate, OA, BC, dust and sea salt. 3 modes: Aitken, accumulation and coarse.
CAM-OSLO (1h)	Kirkevåg et al. (2018)	Köhler theory (κ=1.2 at RH=80 % for sea salt)	Nudged to ERA interim	grid (no)	I, E	sulfate, OA, BC, dust, sea salt (distributed in 12 modes)
GEOS-Chem (1h)	Bey et al. (2001)	GADS and d'Almeida et al. (1991); (g(RH)=2.4 at RH=90 % for sea salt)	GEOS5 version of NASA GMAO	grid (no)	E	sulfate, nitrate, ammonium, BC, and OA (bulk-mass), dust (4), sea salts (2)
GEOS-GOCART (24h)	Chin et al. (2002)	GADS and d'Almeida et al. (1991); (g(RH)=2.4 at RH=90 % for sea salt)	MERRA reanalysis	grid (no)	E	sulfate, BC and OA (2), dust and sea salt (5)
MERRAero (3h)	Buchard et al. (2015)	GADS, d'Almeida et al. (1991) and Tang (1997); (Fig. 1 in Tang (1997))	MERRA reanalysis	grid (no)	E	sulfate, BC and OA (2), dust and sea salt (5)
OsloCTM3 (24h)	Lund et al. (2018)	Fitzgerald (1975). No for BC.	Offline meteorology from IFS ECMWF	grid (no)	I for hydrophilic BC	Primary and secondary OA, BC, sulfate, nitrate, sea salt and dust (8)
TM5 (1h)	van Noije et al. (2014)	Parameterizations in Vignati et al. (2004)	Offline, ERA-Interim	clear-sky (no)	I,E	sulfate, OA, BC, sea salt, dust (7), ammonium nitrate, and MSA
IFS-AER (3h)	Morcrette et al. (2009)	look-up table in Bozzo et al. (2019) (g(RH)=2.36 at RH=90 % for sea salt)	online, initial conditions NWP analysis	grid (no)	E	sea salt (3), dust (3), OA and BC (2)
SALSA (1h)	Kokkola et al. (2018)	Zdanovskii–Stokes–Robinson (ZSR) equation (g(RH)=2.17 for NaCl)	Nudged to ERA interim	clear-sky (no)	E	sulfate, OA, BC, sea salt and dust masses (10)

Note: Most models assume that the hygroscopic growth for inorganic sea salt equals the hygroscopic growth of NaCl ($\kappa \sim 1.5$ at RH=90%), while the κ of inorganic sea salt is closer to ~ 1.1 (see discussion in Zieger et al., 2017).

References

Andrews, E., Sheridan, P. J., Ogren, J. A., Hageman, D., Jefferson, A., Wendell, J., Alástuey, A., Alados-Arboledas, L., Bergin, M., Ealo, M., Hallar, A. G., Hoffer, A., Kalapov, I., Keywood, M., Kim, J., Kim, S.-W., Kolonjari, F., Labuschagne, C., Lin, N.-H., Macdonald, A., Mayol-Bracero, O. L., McCubbin, I. B., Pandolfi, M., Reisen, F., Sharma, S., Sherman, J. P., Sorribas, M., and Sun, J.: Overview of the NOAA/ESRL Federated Aerosol Network, B. Am. Meteorol. Soc., 100, 123–135, https://doi.org/10.1175/BAMS-D-17-0175.1, 2019.

Bergin, M. H., Ogren, J. A., Schwartz, S. E., and McInnes, L. M.: Evaporation of Ammonium Nitrate Aerosol in a Heated Nephelometer: Implications for Field Measurements, Environ. Sci. Technol., 31, 2878–2883, https://doi.org/10.1021/es970089h, 1997.

Bey, I., Jacob, D. J., Yantosca, R. M., Logan, J. A., Field, B. D., Fiore, A. M., Li, Q., Liu, H. Y., Mickley, L. J., and Schultz, M. G.: Global modeling of tropospheric chemistry with assimilated meteorology: Model description and evaluation, J. Geophys. Res.-Atmos., 106, 23 073–23 095, https://doi.org/10.1029/2001JD000807, 2001.

Bian, H., Colarco, P. R., Chin, M., Chen, G., Rodriguez, J. M., Liang, Q., Blake, D., Chu, D. A., da Silva, A., Darmenov, A. S., Diskin, G., Fuelberg, H. E., Huey, G., Kondo, Y., Nielsen, J. E., Pan, X., and Wisthaler, A.: Source attributions of pollution to the Western Arctic during the NASA ARCTAS field campaign, Atmos. Chem. Phys., 13, 4707–4721, https://doi.org/10.5194/acp-13-4707-2013, 2013.

Bian, H., Chin, M., Hauglustaine, D. A., Schulz, M., Myhre, G., Bauer, S. E., Lund, M. T., Karydis, V. A., Kucsera, T. L., Pan, X., Pozzer, A., Skeie, R. B., Steenrod, S. D., Sudo, K., Tsigaridis, K., Tsimpidi, A. P., and Tsyro, S. G.: Investigation of global particulate nitrate from the AeroCom phase III experiment, Atmos. Chem. Phys., 17, 12 911–12 940, https://doi.org/10.5194/acp-17-12911-2017, 2017.

Bond, T. C., Doherty, S. J., Fahey, D. W., Forster, P. M., Berntsen, T., DeAngelo, B. J., Flanner, M. G., Ghan, S., Kärcher, B., Koch, D., et al.: Bounding the role of black carbon in the climate system: A scientific assessment, J. Geophys. Res.-Atmos., 118, 5380–5552, 2013.

Bozzo, A., Benedetti, A., Flemming, J., Kipling, Z., and Rémy, S.: An aerosol climatology for global models based on the tropospheric aerosol scheme in the Integrated Forecasting System of ECMWF, Geosci. Model Dev. Discussion, 2019, 1–35, https://doi.org/10.5194/gmd-2019-149, https://www.geosci-model-dev-discuss.net/gmd-2019-149/, 2019.

Buchard, V., da Silva, A. M., Colarco, P. R., Darmenov, A., Randles, C. A., Govindaraju, R., Torres, O., Campbell, J., and Spurr, R.: Using the OMI aerosol index and absorption aerosol optical depth to evaluate the NASA MERRA Aerosol Reanalysis, Atmos. Chem. Phys., 15, 5743–5760, https://doi.org/10.5194/acp-15-5743-2015, https://www.atmos-chem-phys.net/15/5743/2015/, 2015.

Burgos, M., Andrews, E., Titos, G., Alados-Arboledas, L., Baltensperger, U., Day, D., Jefferson, A., Kalivitis, N., Mihalopoulos, N., Sherman, J., Sun, J., Weingartner, E., and Zieger, P.: A global view on the effect of water uptake on aerosol particle light scattering, Scientific Data, 6, https://doi.org/10.1038/s41597-019-0158-7, 2019.

Chin, M., Ginoux, P., Kinne, S., Torres, O., Holben, B. N., Duncan, B. N., Martin, R. V., Logan, J. A., Higurashi, A., and Nakajima, T.: Tropospheric Aerosol Optical Thickness from the GOCART Model and Comparisons with Satellite and Sun Photometer Measurements, J. Atmos. Sci., 59, 461–483, https://doi.org/10.1175/1520-0469(2002)059<0461:TAOTFT>2.0.CO;2, 2002.

Chin, M., Kahn, R., and Schwartz, S., eds.: Atmospheric Aerosol Properties and Climate Impacts, A Report by the U.S. Climate Change Science Program and the Subcommittee on Global Change Research, National Aeronautics and Space Administration, Washington D.C., U.S.A., 2009.

Colarco, P., da Silva, A., Chin, M., and Diehl, T.: Online simulations of global aerosol distributions in the NASA GEOS-4 model and comparisons to satellite and ground-based aerosol optical depth, J. Geophys. Res.-Atmos., 115, https://doi.org/10.1029/2009JD012820, 2010.

d'Almeida, G., Koepke, P., and Shettle, E.: Atmospheric Aerosols - Global Climatology and Radiative Characteristics, A. Deepak Publishing, 1991.

Dumka, U., Kaskaoutis, D., Sagar, R., Chen, J., Singh, N., and Tiwari, S.: First results from light scattering enhancement factor over central Indian Himalayas during GVAX campaign, Sci. Total Environ., 605, 124–138, 2017.

5   Fierz-Schmidhauser, R., Zieger, P., Vaishya, A., Monahan, C., Bialek, J., O'Dowd, C., Jennings, S., Baltensperger, U., and Weingartner, E.: Light scattering enhancement factors in the marine boundary layer (Mace Head, Ireland), J. Geophys. Res.-Atmos., 115, 2010a.

Fierz-Schmidhauser, R., Zieger, P., Wehrle, G., Jefferson, A., Ogren, J. A., Baltensperger, U., and Weingartner, E.: Measurement of relative humidity dependent light scattering of aerosols, Atmospheric Measurement Techniques, 3, 39–50, https://doi.org/10.5194/amt-3-39-2010, 2010b.

10   Fitzgerald, J. W.: Approximation Formulas for the Equilibrium Size of an Aerosol Particle as a Function of Its Dry Size and Composition and the Ambient Relative Humidity, J. Appl. Meteorol., 14, 1044–1049, https://doi.org/10.1175/1520-0450(1975)014<1044:AFFTES>2.0.CO;2, 1975.

Gerber, H. E.: Relative-humidity parameterization of the Navy Aerosol Model (NAM), Tech. rep., Naval Research Lab Washington DC, 1985.

15   Ghan, S. J., Liu, X., Easter, R. C., Zaveri, R., Rasch, P. J., Yoon, J.-H., and Eaton, B.: Toward a Minimal Representation of Aerosols in Climate Models: Comparative Decomposition of Aerosol Direct, Semidirect, and Indirect Radiative Forcing, J. Climate, 25, 6461–6476, https://doi.org/10.1175/JCLI-D-11-00650.1, 2012.

Gliss, J., Mortier, A., Schulz, M., Andrews, E., Balkanski, Y., Bauer, S., Benedictow, A., Bian, H., Checa-Garcia, R., Chin, M., Ginoux, P., Griesfeller, J., Heckel, A., Holben, B., Kinne, S., Kipling, Z., Kirkevåg, A., Kokkola, H., Laj, P., Le Sager, P., Levy, R., Lund, M., 20   Lund Myhre, C., Matsui, H., Myhre, G., Neubauer, D., Noije, T., North, P., Olivie, D., Sogacheva, L., Takemura, T., Tsigaridis, K., and Tsyro, S.: Multi-model evaluation of modelled aerosol optical properties in the AeroCom Phase III Control experiment using ground and space based columnar observations from AERONET, MODIS, and AATSR and surface in-situ observations from GAW sites, Atmos. Chem. Phys. (in prep.), 2019.

Haywood, J., Bush, M., Abel, S., Claxton, B., Coe, H., Crosier, J., Harrison, M., Macpherson, B., Naylor, M., and Osborne, S.: Prediction of 25   visibility and aerosol within the operational Met Office Unified Model. II: Validation of model performance using observational data, Q. J. Roy. Meteor. Soc., 134, 1817–1832, https://doi.org/10.1002/qj.275, 2008.

Heald, C. L., Ridley, D. A., Kroll, J. H., Barrett, S. R. H., Cady-Pereira, K. E., Alvarado, M. J., and Holmes, C. D.: Contrasting the direct radiative effect and direct radiative forcing of aerosols, Atmos. Chem. Phys., 14, 5513–5527, https://doi.org/10.5194/acp-14-5513-2014, https://www.atmos-chem-phys.net/14/5513/2014/, 2014.

30   Hess, M., Koepke, P., and Schult, I.: Optical properties of aerosols and clouds: The software package OPAC, Bull. Amer. Meteor. Soc., 79, 831–844, 1998.

Hoesly, R. M., Smith, S. J., Feng, L., Klimont, Z., Janssens-Maenhout, G., Pitkanen, T., Seibert, J. J., Vu, L., Andres, R. J., Bolt, R. M., Bond, T. C., Dawidowski, L., Kholod, N., Kurokawa, J.-i., Li, M., Liu, L., Lu, Z., Moura, M. C. P., O'Rourke, P. R., and Zhang, Q.: Historical (1750–2014) anthropogenic emissions of reactive gases and aerosols from the Community Emissions Data System (CEDS), 35   Geosci. Model Dev. (Online), 11, https://doi.org/10.5194/gmd-11-369-2018, 2018.

IPCC: Climate Change 2013: The Physical Science Basis. Contribution of Working Group I to the Fifth Assessment Report of the Intergovernmental Panel on Climate Change, Cambridge University Press Cambridge, UK, and New York, 2013.

Jaeglé, L., Quinn, P. K., Bates, T. S., Alexander, B., and Lin, J.-T.: Global distribution of sea salt aerosols: new constraints from in situ and remote sensing observations, Atmos. Chem. Phys., 11, 3137–3157, https://doi.org/10.5194/acp-11-3137-2011, https://www.atmos-chem-phys.net/11/3137/2011/, 2011.

Jefferson, A., Hageman, D., Morrow, H., Mei, F., and Watson, T.: Seven years of aerosol scattering hygroscopic growth measurements from SGP: Factors influencing water uptake, J. Geophys. Res.-Atmos., 122, 9451–9466, https://doi.org/10.1002/2017JD026804, 2017.

Kinne, S., Schulz, M., Textor, C., Guibert, S., Balkanski, Y., Bauer, S., Berntsen, T., Berglen, T., Boucher, O., Chin, M., Collins, W., Dentener, F., Diehl, T., Easter, R., Feichter, J., Fillmore, D., Ghan, S., Ginoux, P., Gong, S., Grini, A., Hendricks, J., Herzog, M., Horowitz, L., Isaksen, I., Iversen, T., Kirkevåg, A., Kloster, S., Koch, D., Kristjansson, J. E., Krol, M., Lauer, A., Lamarque, J. F., Lesins, G., Liu, X., Lohmann, U., Montanaro, V., Myhre, G., Penner, J., Pitari, G., Reddy, S., Seland, Ø., Stier, P., Takemura, T., and Tie, X.: An AeroCom initial assessment - optical properties in aerosol component modules of global models, Atmos. Chem. Phys., 6, 1815–1834, https://doi.org/10.5194/acp-6-1815-2006, 2006.

Kirkevåg, A., Grini, A., Olivié, D., Seland, Ø., Alterskjær, K., Hummel, M., Karset, I. H. H., Lewinschal, A., Liu, X., Makkonen, R., Bethke, I., Griesfeller, J., Schulz, M., and Iversen, T.: A production-tagged aerosol module for Earth system models, OsloAero5.3 – extensions and updates for CAM5.3-Oslo, Geosci. Model Dev., 11, 3945–3982, https://doi.org/10.5194/gmd-11-3945-2018, 2018.

Kokkola, H., Kühn, T., Laakso, A., Bergman, T., Lehtinen, K. E. J., Mielonen, T., Arola, A., Stadtler, S., Korhonen, H., Ferrachat, S., Lohmann, U., Neubauer, D., Tegen, I., Siegenthaler-Le Drian, C., Schultz, M. G., Bey, I., Stier, P., Daskalakis, N., Heald, C. L., and Romakkaniemi, S.: SALSA2.0: The sectional aerosol module of the aerosol–chemistry–climate model ECHAM6.3.0-HAM2.3-MOZ1.0, Geosci. Model Dev., 11, 3833–3863, https://doi.org/10.5194/gmd-11-3833-2018, https://www.geosci-model-dev.net/11/3833/2018/, 2018.

Köpke, P., Robinson, Hess, I., Schultz, I., and Shettle, E.: Global aerosol data set, Tech. Rep., 243, 44p, 1997.

Liu, X., Easter, R. C., Ghan, S. J., Zaveri, R., Rasch, P., Shi, X., Lamarque, J.-F., Gettelman, A., Morrison, H., Vitt, F., Conley, A., Park, S., Neale, R., Hannay, C., Ekman, A. M. L., Hess, P., Mahowald, N., Collins, W., Iacono, M. J., Bretherton, C. S., Flanner, M. G., and Mitchell, D.: Toward a minimal representation of aerosols in climate models: description and evaluation in the Community Atmosphere Model CAM5, Geosci. Model Dev., 5, 709–739, https://doi.org/10.5194/gmd-5-709-2012, 2012a.

Liu, Y., Key, J. R., Ackerman, S. A., Mace, G. G., and Zhang, Q.: Arctic cloud macrophysical characteristics from CloudSat and CALIPSO, Remote Sens. Environ., 124, 159–173, 2012b.

Lund, M. T., Myhre, G., Haslerud, A. S., Skeie, R. B., Griesfeller, J., Platt, S. M., Kumar, R., Myhre, C. L., and Schulz, M.: Concentrations and radiative forcing of anthropogenic aerosols from 1750 to 2014 simulated with the Oslo CTM3 and CEDS emission inventory, Geosci. Model Dev., 11, 4909–4931, https://doi.org/10.5194/gmd-11-4909-2018, https://www.geosci-model-dev.net/11/4909/2018/, 2018.

Magi, B. I. and Hobbs, P. V.: Effects of humidity on aerosols in southern Africa during the biomass burning season, J. Geophys. Res.-Atmos., 108, https://doi.org/10.1029/2002JD002144, 2003.

Matsui, H.: Development of a global aerosol model using a two-dimensional sectional method: 1. Model design, J. Adv. Model Earth Sy., 9, 1921–1947, https://doi.org/10.1002/2017MS000936, 2017.

Matsui, H. and Mahowald, N.: Development of a global aerosol model using a two-dimensional sectional method: 2. Evaluation and sensitivity simulations, J. Adv. Model Earth Sy., 9, 1887–1920, https://doi.org/10.1002/2017MS000937, 2017.

Matsui, H., Koike, M., Kondo, Y., Fast, J. D., and Takigawa, M.: Development of an aerosol microphysical module: Aerosol Two-dimensional bin module for foRmation and Aging Simulation (ATRAS), Atmos. Chem. Phys., 14, 10 315–10 331, https://doi.org/10.5194/acp-14-10315-2014, 2014.

Metzger, S., Dentener, F., Pandis, S., and Lelieveld, J.: Gas/aerosol partitioning: 1. A computationally efficient model, J. Geophys. Res.-Atmos., 107, ACH 16–1–ACH 16–24, https://doi.org/10.1029/2001JD001102, 2002.

Morcrette, J.-J., Boucher, O., Jones, L., Salmond, D., Bechtold, P., Beljaars, A., Benedetti, A., Bonet, A., Kaiser, J. W., Razinger, M., Schulz, M., Serrar, S., Simmons, A. J., Sofiev, M., Suttie, M., Tompkins, A. M., and Untch, A.: Aerosol analysis and forecast in the European Centre for Medium-Range Weather Forecasts Integrated Forecast System: Forward modeling, J. Geophys. Res.-Atmos., 114, https://doi.org/10.1029/2008JD011235, 2009.

Myhre, G., Bellouin, N., Berglen, T. F., Berntset, T. K., Boucher, O., Grini, A., Isaken, I. S. A., Johnsrud, M., Mishchenko, M. I., Stordal, F., and Tanré, D.: Comparison of the radiative properties and direct radiative effect of aerosols from a global aerosol model and remote sensing data over ocean, Tellus B, 59, 115–129, https://doi.org/10.1111/j.1600-0889.2006.00226.x, 2007.

Myhre, G., Samset, B. H., Schulz, M., Balkanski, Y., Bauer, S., Berntsen, T. K., Bian, H., Bellouin, N., Chin, M., Diehl, T., Easter, R. C., Feichter, J., Ghan, S. J., Hauglustaine, D., Iversen, T., Kinne, S., Kirkevåg, A., Lamarque, J.-F., Lin, G., Liu, X., Lund, M. T., Luo, G., Ma, X., van Noije, T., Penner, J. E., Rasch, P. J., Ruiz, A., Seland, Ø., Skeie, R. B., Stier, P., Takemura, T., Tsigaridis, K., Wang, P., Wang, Z., Xu, L., Yu, H., Yu, F., Yoon, J.-H., Zhang, K., Zhang, H., and Zhou, C.: Radiative forcing of the direct aerosol effect from AeroCom Phase II simulations, Atmos. Chem. Phys., 13, 1853–1877, https://doi.org/10.5194/acp-13-1853-2013, 2013.

Peng, C., Chan, M. N., and Chan, C. K.: The Hygroscopic Properties of Dicarboxylic and Multifunctional Acids: Measurements and UNIFAC Predictions, Environ. Sci. Technol., 35, 4495–4501, https://doi.org/10.1021/es0107531, 2001.

Ramanathan, V., Crutzen, P., Kiehl, J., and Rosenfeld, D.: Aerosols, climate and the hydrological cycle, Science, 294, 2119–2124, 2001.

Regayre, L. A., Johnson, J. S., Yoshioka, M., Pringle, K. J., Sexton, D. M. H., Booth, B. B. B., Lee, L. A., Bellouin, N., and Carslaw, K. S.: Aerosol and physical atmosphere model parameters are both important sources of uncertainty in aerosol ERF, Atmos. Chem. Phys., 18, 9975–10 006, https://doi.org/10.5194/acp-18-9975-2018, https://www.atmos-chem-phys.net/18/9975/2018/, 2018.

Rémy, S., Kipling, Z., Flemming, J., Boucher, O., Nabat, P., Michou, M., Bozzo, A., Ades, M., Huijnen, V., Benedetti, A., Engelen, R., Peuch, V.-H., and Morcrette, J.-J.: Description and evaluation of the tropospheric aerosol scheme in the Integrated Forecasting System (IFS-AER, cycle 45R1) of ECMWF, Geosci. Model Dev. Discussions, 2019, 1–50, https://doi.org/10.5194/gmd-2019-142, 2019.

Rienecker, M. M., Suarez, M. J., Gelaro, R., Todling, R., Bacmeister, J., Liu, E., Bosilovich, M. G., Schubert, S. D., Takacs, L., Kim, G.-K., Bloom, S., Chen, J., Collins, D., Conaty, A., da Silva, A., Gu, W., Joiner, J., Koster, R. D., Lucchesi, R., Molod, A., Owens, T., Pawson, S., Pegion, P., Redder, C. R., Reichle, R., Robertson, F. R., Ruddick, A. G., Sienkiewicz, M., and Woollen, J.: MERRA: NASA's Modern-Era Retrospective Analysis for Research and Applications, J. Climate, 24, 3624–3648, https://doi.org/10.1175/JCLI-D-11-00015.1, 2011.

Schulz, M., Textor, C., Kinne, S., Balkanski, Y., Bauer, S., Berntsen, T., Berglen, T., Boucher, O., Dentener, F., Guibert, S., Isaksen, I., Iversen, T., Koch, D., Kirkevåg, A., Liu, X., Montanaro, V., Myhre, G., Penner, J., Pitari, G., Reddy, S., Seland, Ø., Stier, P., and Takemura, T.: Radiative forcing by aerosols as derived from the AeroCom present-day and pre-industrial simulations, Atmos. Chem. Phys., 6, 5225–5246, https://doi.org/10.5194/acp-6-5225-2006, 2006.

Schutgens, N. A. J., Partridge, D. G., and Stier, P.: The importance of temporal collocation for the evaluation of aerosol models with observations, Atmos. Chem. Phys., 16, 1065–1079, https://doi.org/10.5194/acp-16-1065-2016, 2016.

Sheridan, P., Delene, D., and Ogren, J.: Four years of continuous surface aerosol measurements from the Department of Energy's Atmospheric Radiation Measurement Program Southern Great Plains Cloud and Radiation Testbed site, J. Geophys. Res., 106, 20 735–20 747, 2001.

Sjogren, S., Gysel, M., Weingartner, E., Baltensperger, U., Cubison, M., Coe, H., Zardini, A., Marcolli, C., Krieger, U., and Peter, T.: Hygroscopic growth and water uptake kinetics of two-phase aerosol particles consisting of ammonium sulfate, adipic and humic acid mixtures, J. Aerosol Sci., 38, 157–171, 2007.

Søvde, O. A., Prather, M. J., Isaksen, I. S. A., Berntsen, T. K., Stordal, F., Zhu, X., Holmes, C. D., and Hsu, J.: The chemical transport model Oslo CTM3, Geosci. Model Dev., 5, 1441–1469, https://doi.org/10.5194/gmd-5-1441-2012, https://www.geosci-model-dev.net/5/1441/2012/, 2012.

Stokes, R. H. and Robinson, R. A.: Interactions in Aqueous Nonelectrolyte Solutions. I. Solute-Solvent Equilibria, J. Phys. Chem., 70, 2126–2131, https://doi.org/10.1021/j100879a010, 1966.

Tang, I. N.: Thermodynamic and optical properties of mixed-salt aerosols of atmospheric importance, J. Geophys. Res.-Atmos., 102, 1883–1893, https://doi.org/10.1029/96JD03085, 1997.

Tang, I. N. and Munkelwitz, H. R.: Water activities, densities, and refractive indices of aqueous sulfates and sodium nitrate droplets of atmospheric importance, J. Geophys. Res.-Atmos., 99, 18 801–18 808, https://doi.org/10.1029/94JD01345, 1994.

Taylor, K. E.: Summarizing multiple aspects of model performance in a single diagram, J. Geophys. Res.-Atmos., 106, 7183–7192, https://doi.org/10.1029/2000JD900719, 2001.

Textor, C., Schulz, M., Guibert, S., Kinne, S., Balkanski, Y., Bauer, S., Berntsen, T., Berglen, T., Boucher, O., Chin, M., Dentener, F., Diehl, T., Easter, R., Feichter, H., Fillmore, D., Ghan, S., Ginoux, P., Gong, S., Grini, A., Hendricks, J., Horowitz, L., Huang, P., Isaksen, I., Iversen, I., Kloster, S., Koch, D., Kirkevåg, A., Kristjansson, J. E., Krol, M., Lauer, A., Lamarque, J. F., Liu, X., Montanaro, V., Myhre, G., Penner, J., Pitari, G., Reddy, S., Seland, Ø., Stier, P., Takemura, T., and Tie, X.: Analysis and quantification of the diversities of aerosol life cycles within AeroCom, Atmos. Chem. Phys., 6, 1777–1813, https://doi.org/10.5194/acp-6-1777-2006, 2006.

Textor, C., Schulz, M., Guibert, S., Kinne, S., Balkanski, Y., Bauer, S., Berntsen, T., Berglen, T., Boucher, O., Chin, M., Dentener, F., Diehl, T., Feichter, J., Fillmore, D., Ginoux, P., Gong, S., Grini, A., Hendricks, J., Horowitz, L., Huang, P., Isaksen, I., Iversen, T., Kloster, S., Koch, D., Kirkevåg, A., Kristjansson, J., Krol, M., Lauer, A., Lamarque, J., Liu, X., Montanaro, V., Myhre, G., Penner, J. E., Pitari, G., Reddy, M. S., Seland, Ø., Stier, P., Takemura, T., and Tie, X.: The effect of harmonized emissions on aerosol properties in global models – an AeroCom experiment, Atmos. Chem. Phys., 7, 4489–4501, https://doi.org/10.5194/acp-7-4489-2007, 2007.

Titos, G., Jefferson, A., Sheridan, P. J., Andrews, E., Lyamani, H., Alados-Arboledas, L., and Ogren, J. A.: Aerosol light-scattering enhancement due to water uptake during the TCAP campaign, Atmos. Chem. Phys., 14, 7031–7043, https://doi.org/10.5194/acp-14-7031-2014, 2014.

Titos, G., Cazorla, A., Zieger, P., Andrews, E., Lyamani, H., Granados-Muñoz, M., Olmo, F., and Alados-Arboledas, L.: Effect of hygroscopic growth on the aerosol light-scattering coefficient: A review of measurements, techniques and error sources, Atmos. Environ., 141, 494 – 507, https://doi.org/https://doi.org/10.1016/j.atmosenv.2016.07.021, 2016.

Titos, G., del Águila, A., Cazorla, A., Lyamani, H., Casquero-Vera, J., Colombi, C., Cuccia, E., Gianelle, V., Močnik, G., Alastuey, A., Olmo, F., and Alados-Arboledas, L.: Spatial and temporal variability of carbonaceous aerosols: Assessing the impact of biomass burning in the urban environment, Sci. Total Environ., 578, 613 – 625, https://doi.org/https://doi.org/10.1016/j.scitotenv.2016.11.007, 2017.

van Noije, T. P. C., Le Sager, P., Segers, A. J., van Velthoven, P. F. J., Krol, M. C., Hazeleger, W., Williams, A. G., and Chambers, S. D.: Simulation of tropospheric chemistry and aerosols with the climate model EC-Earth, Geosci. Model Dev., 7, 2435–2475, https://doi.org/10.5194/gmd-7-2435-2014, https://www.geosci-model-dev.net/7/2435/2014/, 2014.

Vignati, E., Wilson, J., and Stier, P.: M7: An efficient size-resolved aerosol microphysics module for large-scale aerosol transport models, J. Geophys. Res.-Atmos., 109, https://doi.org/10.1029/2003JD004485, 2004.

Wang, W., Rood, M., Carrico, C., Covert, D., Quinn, P., and Bates, T.: Aerosol optical properties along the northeast coast of North America during the New England Air Quality Study–Intercontinental Transport and Chemical Transformation 2004 campaign and the influence of aerosol composition, J. Geophys. Res.-Atmos., 112, https://doi.org/10.1029/2006JD007579, 2007.

Weingartner, E., Baltensperger, U., and Burtscher, H.: Growth and structural change of combustion aerosols at high relative humidity, Environ. Sci. Technol., 29, 2982–2986, 1995.

WMO/GAW: WMO/GAW Aerosol Measurement Procedures, Guidelines and Recommendations, Report No. 227, World Meteorological Organization, Geneva, Switzerland, 2nd edition edn., 2016.

Zdanovskii, A.: Novyi Metod Rascheta Rastvorimostei Electrolitov V Mnogokompenentnykh sistemakh .1., Zhurnal Fizichekoi Khimii, 22, 1478–1485, 1948.

Zeleznik, F.: Thermodynamic properties of the aqueous sulfuric acid system to 350 K, J. Phys. Chem. Ref. Data, 20, 1157–1200, 1991.

Zhang, K., O'Donnell, D., Kazil, J., Stier, P., Kinne, S., Lohmann, U., Ferrachat, S., Croft, B., Quaas, J., Wan, H., Rast, S., and Feichter, J.: The global aerosol-climate model ECHAM-HAM, version 2: sensitivity to improvements in process representations, Atmos. Chem. Phys., 12, 8911–8949, https://doi.org/10.5194/acp-12-8911-2012, http://www.atmos-chem-phys.net/12/8911/2012/, 2012.

Zhang, K., Wan, H., Liu, X., Ghan, S. J., Kooperman, G. J., Ma, P.-L., Rasch, P. J., Neubauer, D., and Lohmann, U.: Technical Note: On the use of nudging for aerosolâ€"climate model intercomparison studies, Atmos. Chem. Phys., 14, 8631–8645, https://doi.org/10.5194/acp-14-8631-2014, 2014.

Zhang, L., Sun, J. Y., Shen, X. J., Zhang, Y. M., Che, H., Ma, Q. L., Zhang, Y. W., Zhang, X. Y., and Ogren, J. A.: Observations of relative humidity effects on aerosol light scattering in the Yangtze River Delta of China, Atmos. Chem. Phys., 15, 8439–8454, https://doi.org/10.5194/acp-15-8439-2015, 2015.

Zieger, P., Fierz-Schmidhauser, R., Gysel, M., Ström, J., Henne, S., Yttri, K., Baltensperger, U., and Weingartner, E.: Effects of relative humidity on aerosol light scattering in the Arctic, Atmos. Chem. Phys., 10, 3875–3890, https://doi.org/10.5194/acp-10-3875-2010, 2010.

Zieger, P., Fierz-Schmidhauser, R., Weingartner, E., and Baltensperger, U.: Effects of relative humidity on aerosol light scattering: results from different European sites, Atmos. Chem. Phys., 13, 10 609–10 631, https://doi.org/10.5194/acp-13-10609-2013, http://www.atmos-chem-phys.net/13/10609/2013/, 2013.

Zieger, P., Fierz-Schmidhauser, R., Poulain, L., Müller, T., Birmili, W., Spindler, G., Wiedensohler, A., Baltensperger, U., and Weingartner, E.: Influence of water uptake on the aerosol particle light scattering coefficients of the Central European aerosol, Tellus B: Chemical and Physical Meteorology, 66, 22 716, 2014.

Zieger, P., Aalto, P. P., Aaltonen, V., Äijälä, M., Backman, J., Hong, J., Komppula, M., Krejci, R., Laborde, M., Lampilahti, J., de Leeuw, G., Pfüller, A., Rosati, B., Tesche, M., Tunved, P., Väänänen, R., and Petäjä, T.: Low hygroscopic scattering enhancement of boreal aerosol and the implications for a columnar optical closure study, Atmos. Chem. Phys., 15, 7247–7267, https://doi.org/10.5194/acp-15-7247-2015, https://www.atmos-chem-phys.net/15/7247/2015/, 2015.

Zieger, P., Väisänen, O., Corbin, J., Partridge, D. G., Bastelberger, S., Mousavi-Fard, M., Rosati, B., Gysel, M., Krieger, U., Leck, C., Nenes, A., Riipinen, I., Virtanen, A., and Salter, M.: Revising the hygroscopicity of inorganic sea salt particles, Nat. Commun., 8, https://doi.org/10.1038/ncomms15883, 2017.
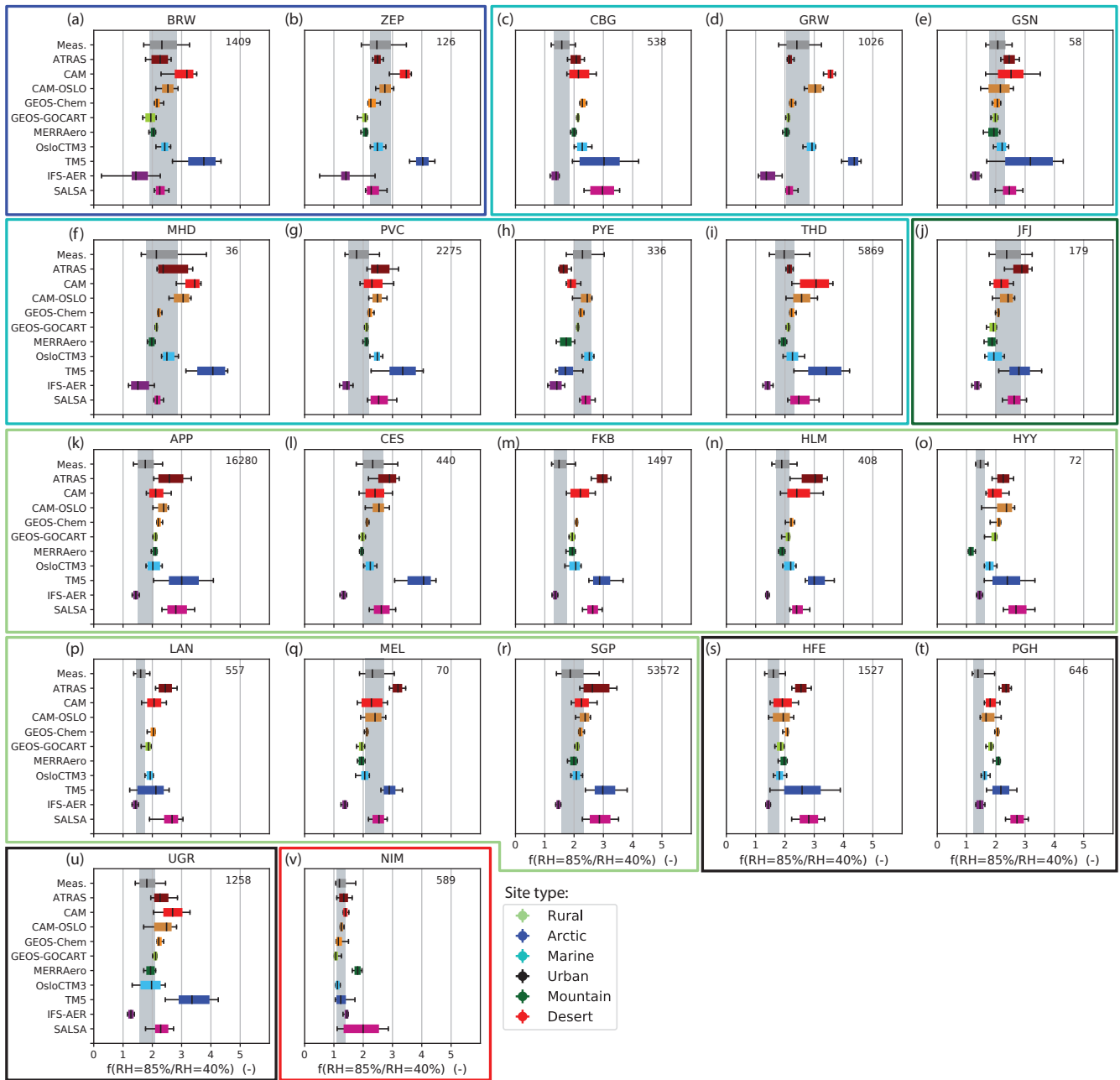
Figure 1. The scattering enhancement f(RH=85 %/RH$_{ref}$=40 %) at $\lambda = 550$ nm as measured and predicted by the various models for all investigated sites (panel **(a)** - **(v)**). The box edges represent the 25th to the 75th percentile (the gray underlying area represents the quartiles for all measurements), with the center line indicating the median. The whiskers show the range of the data extending from the percentiles 10th to 90th. The number in the top right corner indicates the number of available measurements at each site (temporal resolution shown in Table 1). The colored boxes grouping the different sets of plots indicate the site type.
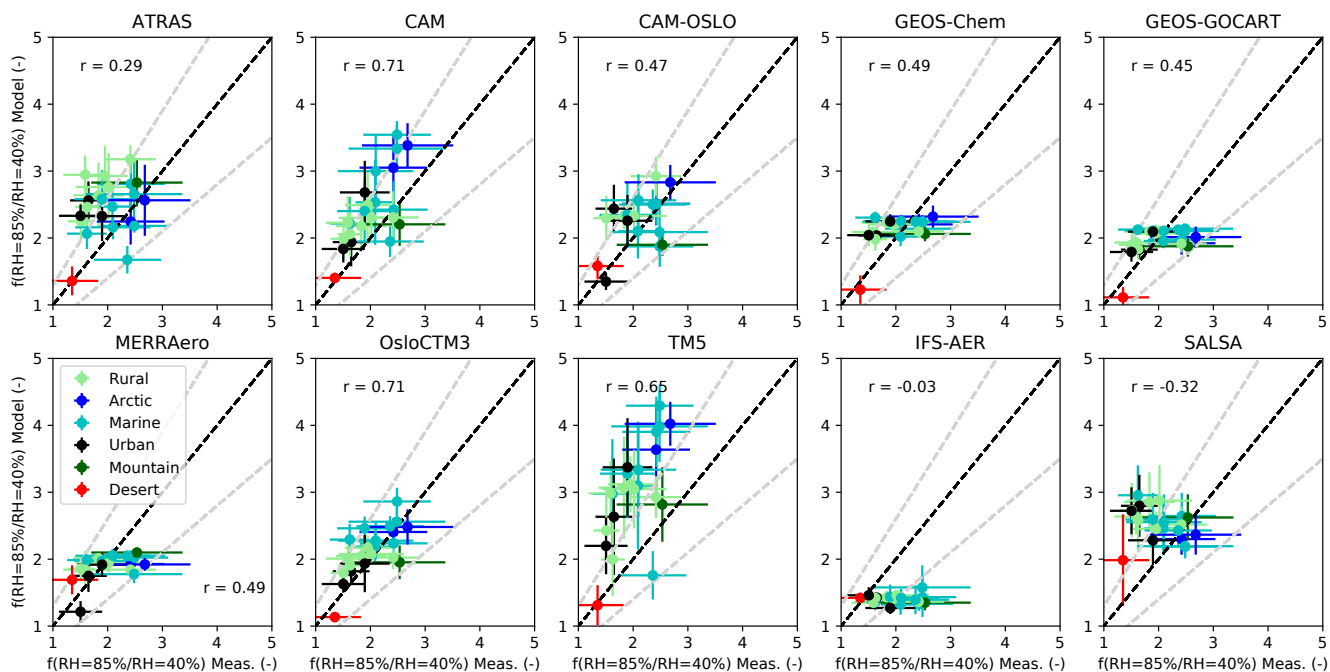
Figure 2. Predicted versus measured f(RH=85 %/RH$_{ref}$=40 %) at $\lambda = 550$ nm for each model color-coded by site type: blue for Arctic, cyan for marine, dark green for mountain, light green for rural, black for urban, and red for desert sites (panel **(a)** - **(j)**). The Pearson correlation coefficient (r) is indicated for each panel. The dashed black line shows the 1:1-line and gray dashed line shows the upper estimate of measurement uncertainties.
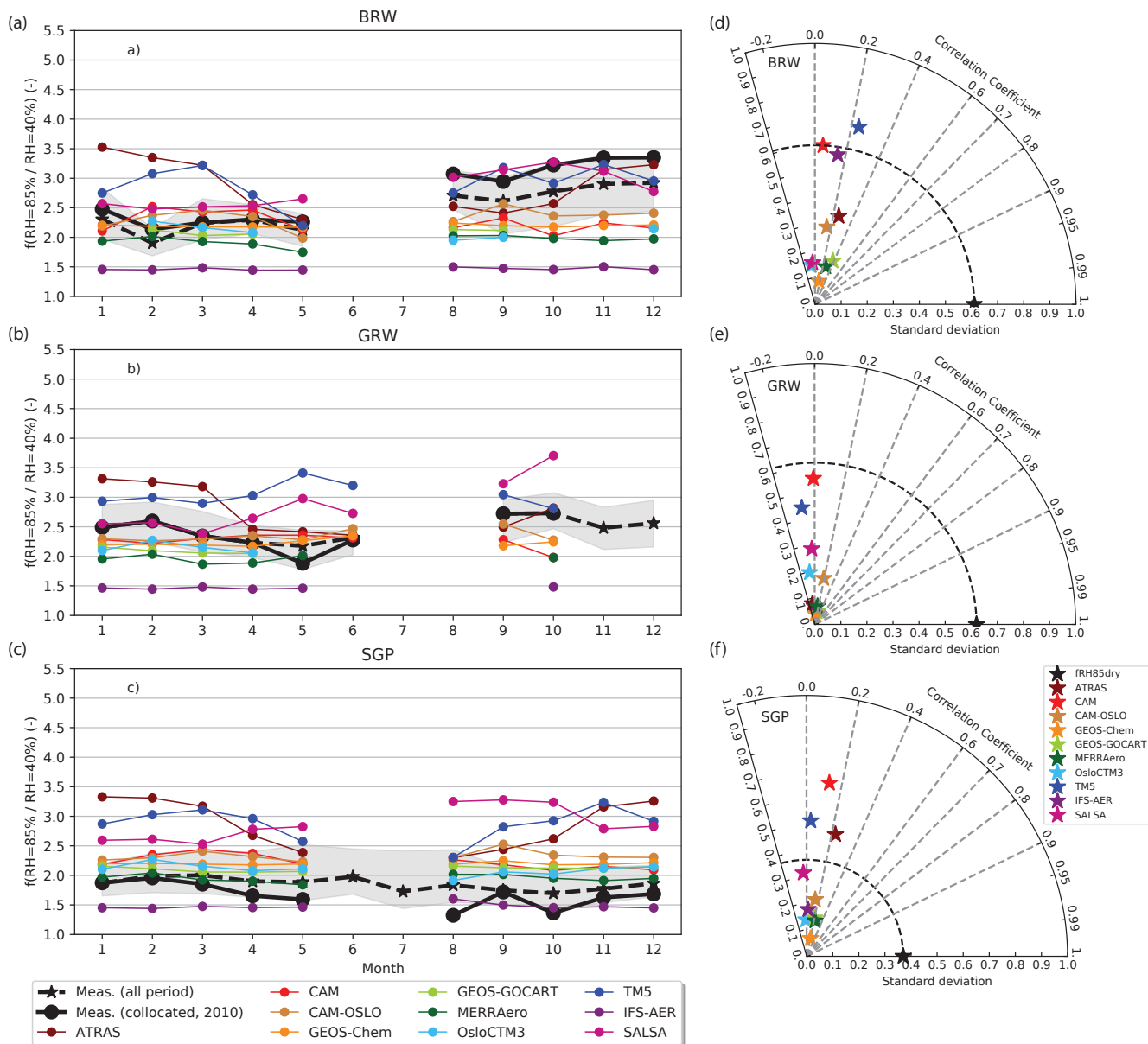
Figure 3. Comparison of $f(\text{RH}=85\,\%/\text{RH}_{\text{ref}}=40\,\%)$ at $\lambda = 550\,\text{nm}$ with temporally collocated data for 2010: Barrow (Arctic site), Graciosa (marine site), and Southern Great Plains (rural site). **(a)-(c)** Annual cycles of the median $f(\text{RH}=85\,\%/\text{RH}_{\text{ref}}=40\,\%)$ as measured (black line) and as predicted by the models (colored lines) collocated for 2010. The black dashed line and gray underlying area represent the median and range for the entire dataset. **(d)-(f)** Taylor diagrams showing the correlation coefficients and standard deviations of $f(\text{RH}=85\,\%/\text{RH}_{\text{ref}}=40\,\%)$ for measurements (black symbols) and models (colored symbols, see legend).
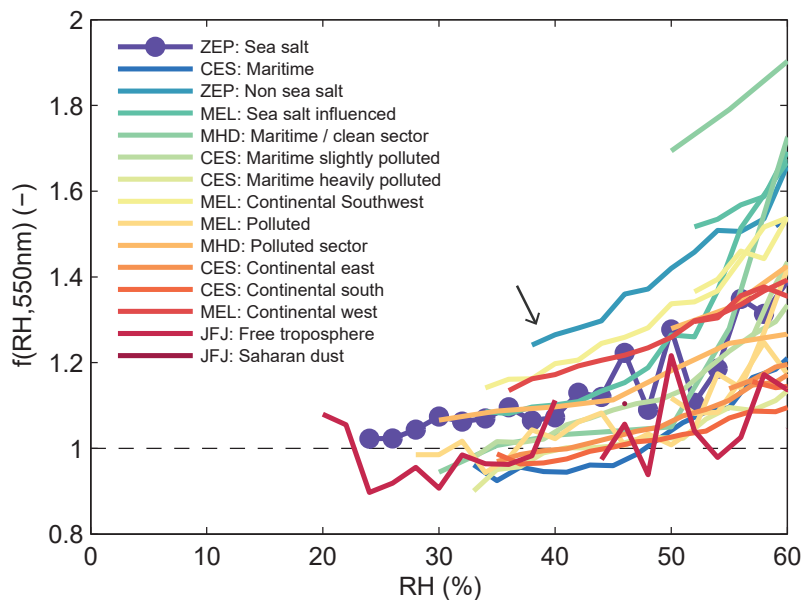
Figure 4. Scattering enhancement vs. relative humidity for different aerosol types measured at various European sites using a tandem nephelometer humidograph system (taken from Zieger et al., 2013). Lines are color coded from clean/maritime air masses (blue lines) to polluted/dust air masses (red lines). The curve for the pristine sea salt dominated event measured at Ny-Ålesund, in the Arctic (blue dots), follows the behavior of pure inorganic sea salt, which would also exhibit hysteresis effects (see Fig. S4 in the supplement).
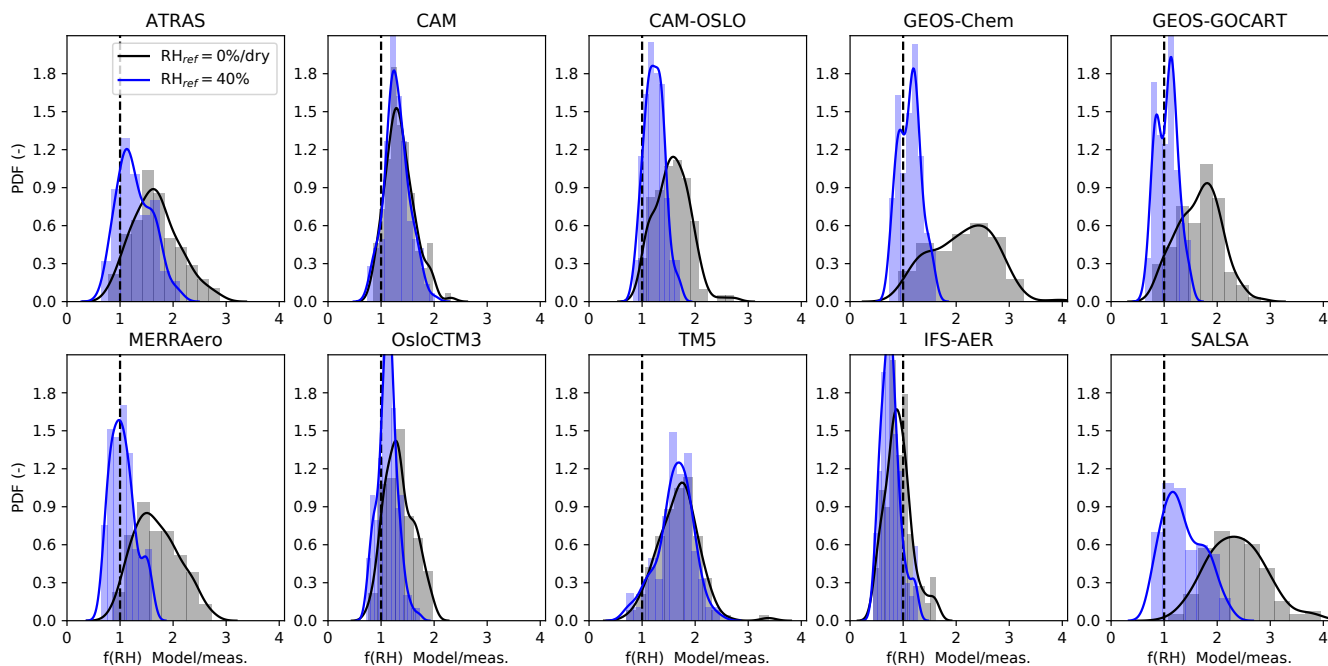
Figure 5. Probability density functions of the ratio $f(\mathrm{RH})_{\mathrm{model}}/f(\mathrm{RH})_{\mathrm{meas.}}$ for all sites for each model. The blue values denote the ratios if RH=40 % is taken as reference RH. The gray areas represent the ratio if $\mathrm{RH}_{\mathrm{ref}}$=0 % (models) or $\mathrm{RH}_{\mathrm{ref}}$=dry (measurements) is taken.

.